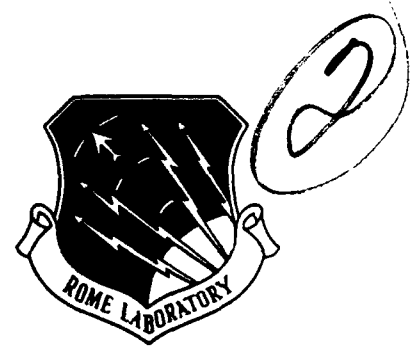


AD-A248 573



RL-TR-91-377
Final Technical Report
December 1991



INTEGRATED OPTICAL PIPELINED POLYNOMIAL PROCESSORS

Georgia Institute of Technology

Carl Verber



APPROVED FOR PUBLIC RELEASE; DISTRIBUTION UNLIMITED.

92-09599



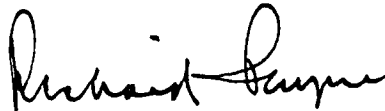
02 4 14 029

Rome Laboratory
Air Force Systems Command
Griffiss Air Force Base, NY 13441-5700

This report has been reviewed by the Rome Laboratory Public Affairs Division (PA) and is releasable to the National Technical Information Service (NTIS). At NTIS it will be releasable to the general public, including foreign nations.

RL-TR-91-377 has been reviewed and is approved for publication.

APPROVED:



RICHARD PAYNE, Chief
Electro-Optical Device Tech Division

FOR THE COMMANDER:



HAROLD ROTH, Director
Solid State Sciences Directorate

If your address has changed or if you wish to be removed from the Rome Laboratory mailing list, or if the addressee is no longer employed by your organization, please notify Rome Laboratory (ERO) Hanscom AFB MA 01731-5000. This will assist us in maintaining a current mailing list.

Do not return copies of this report unless contractual obligations or notices on a specific document require that it be returned.

REPORT DOCUMENTATION PAGE

Form Approved
OMB No. 0704-0188

Public reporting burden for this collection of information is estimated to average 1 hour per response, including the time for reviewing instructions, searching existing data sources, gathering and maintaining the data needed, and completing and reviewing the collection of information. Send comments regarding this burden estimate or any other aspect of this collection of information, including suggestions for reducing this burden, to Washington Headquarters Services, Directorate for Information Operations and Reports, 1215 Jefferson Davis Highway, Suite 1204, Arlington, VA 22202-4302, and to the Office of Management and Budget, Paperwork Reduction Project (0704-0188), Washington, DC 20503.

1. AGENCY USE ONLY (Leave Blank)		2. REPORT DATE December 1991		3. REPORT TYPE AND DATES COVERED Final May 85 - Apr 89	
4. TITLE AND SUBTITLE INTEGRATED OPTICAL PIPELINED POLYNOMIAL PROCESSORS				5. FUNDING NUMBERS C - F19628-86-K-0133 PE - 62702F PR - 4600 TA - 19 WU - 57	
6. AUTHOR(S) Carl Verber					
7. PERFORMING ORGANIZATION NAME(S) AND ADDRESS(ES) Georgia Institute of Technology School of Electrical Engineering Atlanta GA 30332				8. PERFORMING ORGANIZATION REPORT NUMBER N/A	
9. SPONSORING/MONITORING AGENCY NAME(S) AND ADDRESS(ES) Rome Laboratory (ERO) Hanscom AFB MA 01731-5000				10. SPONSORING/MONITORING AGENCY REPORT NUMBER RL-TR-91-377	
11. SUPPLEMENTARY NOTES Rome Laborator Project Engineer: Philip R. Hemmer/ERO/(617) 377-5170					
12a. DISTRIBUTION/AVAILABILITY STATEMENT Approved for public release; distribution unlimited.				12b. DISTRIBUTION CODE	
13. ABSTRACT (Maximum 200 words) The purpose of this research was to design, fabricate and characterize a high speed integrated optical pipelined polynomial processor capable of evaluating square roots and solving polynomials up to third order. The Horner rule for polynomial evaluation was applied. The fabricated test devices consisted of a line of alternating adder and multiplier gratings deposited on a single chip of LiNbO3. Both adder and multiplier gratings were electro-optic. The coefficients of the polynomial to be evaluated were input as voltages to the adder gratings, while the variables were scanned by applying a ramp voltage to the multiplier gratings. To evaluate square roots, a second order polynomial was solved. The square root device performed approximately as predicted by the design equations. The third order polynomial evaluator, however, did not perform as predicted, due to a design error. This error was corrected and new devices were fabricated. These new devices performed as predicted and also incorporated significant design improvements, based on the test results of the first devices.					
14. SUBJECT TERMS Integrated Optics, Square Root Evaluator				15. NUMBER OF PAGES 76	
				16. PRICE CODE	
17. SECURITY CLASSIFICATION OF REPORT UNCLASSIFIED	18. SECURITY CLASSIFICATION OF THIS PAGE UNCLASSIFIED	19. SECURITY CLASSIFICATION OF ABSTRACT UNCLASSIFIED	20. LIMITATION OF ABSTRACT UL		

TABLE OF CONTENTS

LIST OF TABLES	5
LIST OF FIGURES	6
INTRODUCTION	8
<u>ORIGINALLY-PROPOSED DEVICE CONCEPT</u>	8
<u>CHANNEL-GUIDE ALTERNATIVE LAYOUT</u>	12
OVERALL SYSTEM CONSIDERATIONS	14
<u>Diffraction Limit</u>	14
<u>GRATING CONSIDERATIONS</u>	14
<u>Basic Grating Equations</u>	14
<u>Bragg Regime Diffraction Criteria</u>	15
<u>Grating Requirements</u>	15
<u>Laser Characteristics</u>	17
<u>Lens Characteristics</u>	18
<u>Substrate Orientation</u>	18
DESIGN CONSIDERATIONS	20
<u>DESIGN LAYOUT OPTIONS</u>	20
<u>Option 1:</u>	20
<u>Option 2:</u>	22
<u>OPTION 1 ANGULAR RELATIONS</u>	22
<u>OPTION 2 ANGULAR RELATIONS</u>	25
<u>Case 1</u>	25
<u>Case 2</u>	27
DESIGN OF THE PHOTOMASK	28
<u>SELECTION OF GRATING PARAMETERS</u>	28

<u>Selection of Grating Periods</u>	28
<u>MANAGEMENT OF UNDIFFRACTED BEAMS</u>	29
<u>Coefficient Beams</u>	31
<u>Undiffracted Coefficient Beams</u>	31
<u>Signal Beam</u>	31
<u>Undiffracted Signal Beams</u>	31
<u>Re-diffraction of Stray Beams</u>	32
<u>Adder Gratings</u>	32
<u>Multiplier Gratings</u>	33
<u>DESIGN CONSTRAINTS: LAYOUT</u>	33
<u>Adder Gratings</u>	33
<u>Multiplier Gratings</u>	34
FABRICATION ISSUES	35
<u>PRELIMINARY FABRICATION STUDIES</u>	35
<u>Grating Evaluation Experiments</u>	35
<u>Processor Waveguide Fabrication</u>	36
<u>Modulator Fabrication and Evaluation</u>	37
<u>Modulator Fabrication</u>	37
<u>Sample Characterization</u>	39
<u>PROCESSOR EVALUATION</u>	39
<u>ANISOTROPIC DIFFRACTION</u>	43
<u>FABRICATION ON Z-CUT SUBSTRATES</u>	46
<u>EVALUATION OF Z-CUT PROCESSORS</u>	46
IMPLEMENTATION OF SQUARE-ROOT PROCESSOR	50
<u>INTRODUCTION</u>	50
<u>EXPERIMENTAL SETUP</u>	50
<u>EXPERIMENTAL RESULTS</u>	54
RE-DESIGN FOR Y-CUT CRYSTALS	61

<u>DESIGN TRADEOFFS</u>	61
<u>Selection of y-Cut Crystals</u>	61
<u>Propagation Direction and Polarization</u>	61
<u>Anisotropic Diffraction</u>	62
<u>REDESIGN PARAMETERS</u>	62
<u>The Redesign Process</u>	63
<u>New Design Parameters</u>	63
<u>FABRICATION OF NEW PROCESSOR SAMPLES</u>	63
 LIST OF SYMBOLS	 66
 REFERENCES	 67

Accession For	
NTIS GRA&I	<input checked="" type="checkbox"/>
DTIC TAB	<input type="checkbox"/>
Unannounced	<input type="checkbox"/>
Justification	
By	
Distribution/	
Availability Codes	
Dist	Avail and/or Special
A-1	

LIST OF TABLES

Table I. Data for Sharp Laser Diodes	17
Table II. Summary of System Choices	20
Table III. Final Device Parameters	30
Table IV. Fixed Surface Grating Sample Parameters	35
Table V. Results of Diffraction Grating Experiments	36
Table VI. Electrode Delineation Procedure	39
Table VII. Measured Mode Indices for Planar Optical Waveguides	41
Table VIII. Measured Bragg Angles and Angular Misalignments	45
Table IX. Fabrication Parameters for Pipelined Polynomial Processor	47
Table X. Final Device Parameters	65

LIST OF FIGURES

Figure 1. Schematic of original processor concept, using holographic surface gratings for adders and electrooptic overlap gratings for multipliers.	9
Figure 2. Illustration of grating types. (a) an overlap grating; (b) a Kogelnik grating. The output beam boundaries are emphasized.	11
Figure 3. Schematic of a channelized version of the processor, using directional coupler modulators for light switching.	13
Figure 4. (a) Geometry used to calculate the collimation error associated with a lens fabrication error ϵ ; (b) details showing angular relations.	19
Figure 5. Schematic illustration of Option 1 for the processor layout.	21
Figure 6. Schematic illustration of Option 2 for the processor layout.	23
Figure 7. Angular Relations for Option 1, Odd Adders or Option 2, Case 1, Odd Adders (Reflect in SA for Even Adders).	24
Figure 8. Angular Relations for Option 1, Even Adders or Option 2, Case 2, Odd Adders (Reflect in SA for Even Adders).	26
Figure 9. Mode Plots for Z-cut Lithium Niobate Waveguide ($\lambda = 632.8$ nm; Ti thickness = 250Å; diffusion time = 5 hours; diffusion temperature = 1000°C).	38
Figure 10. Diffraction efficiency plots for modulator gratings.	40
Figure 11. Diffraction efficiency of an adder grating at a wavelength of 632.8 nm . .	42
Figure 12. Schematic representation of light propagating through two adjacent electrooptic modulators. Perfect angular alignment will result in simultaneous diffraction by gratings A_2 and M_2	44
Figure 13. Images of diffracted and undiffracted light from two adjacent modulators. (a) 0 V on A_1 , 15 V on M_2 ; (b) 50 V on A_1 , 15 V on M_2	49
Figure 14. Spatial layout of PPZ-4 device. S_1 denotes the input laser beam, M_1 and M_2 denote the multiplier gratings, and A_1 denotes the adder grating. . .	51
Figure 15. Waveform generated by the function generator to drive the multiplier gratings. The horizontal trace at the bottom of the figure is the zero voltage level. Note the section of the curve at the far left of the trace. . . .	53
Figure 16. The laboratory setup used in the experiments.	55

Figure 17. The undiffracted zeroth and first diffracted orders for the three gratings are shown. The subscripts (ij) associated with the beams on the screen represent the grating (i) and diffraction order (j) that the beam represents.	56
Figure 18. Oscilloscope trace of beam A_{11} (or M_{20}) with grating M_2 turned off. The horizontal trace in the figure represents the zero level.	57
Figure 19. Oscilloscope trace of the first diffracted order from the second multiplier grating. The ringing at the left is due to the detector. Lower trace: zero-voltage level.	58
Figure 20. Simplified layout of square root experiment. The a_1x^2 output of the device is detected and input to the comparator circuit where it is compared to a known d.c. voltage. The output of the comparator is displayed on an oscilloscope.	59
Figure 21. Oscilloscope trace showing adjustment of the d.c. level to set the zero of the output signal.	60

INTRODUCTION

The objective of this program was to design, fabricate and characterize laboratory versions of a high-speed, integrated-optic pipelined processor for evaluation of polynomial functions. The program was carried out with the design and characterization portions performed at Georgia Tech and the fabrication performed at Battelle-Columbus Laboratories, Columbus, Ohio.

The concept of a Pipelined Polynomial Processor was first proposed by Verber *et al*¹; this proposal included methods for implementing negative coefficients and negative or complex solutions. This was later elaborated by Kenan and Verber², where some applications are discussed and design issues are brought forward. In particular, the issues of the scaling of argument and coefficients are addressed along with questions about electronic support.

ORIGINALLY-PROPOSED DEVICE CONCEPT

The originally-proposed device is pictured schematically in Figure 1. In this device, the polynomial

$$\begin{aligned} P_N(x) &= a_N x^N + a_{N-1} x^{N-1} + \dots + a_1 x + a_0 \\ &= (a_N x + a_{N-1}(x + a_{N-2}(x + \dots + a_1(x + a_0)))) \dots \end{aligned} \quad (1)$$

is to be evaluated using the synthetic division factorization indicated on the second line, which breaks the evaluation into a series of "multiply by x, then add an a" steps suitable for pipelining. The coefficients a_i are introduced by modulation of independent, mutually-incoherent*, laser diodes. The coefficient inputs are combined with the signal already progressing through the device by surface gratings which we will call "adder" gratings. The argument of the polynomial, x, is introduced through N electrooptic gratings, which we will call "multiplier" gratings.

For discussions of architecture, this layout is adequate. However, this design is impractical for actual implementation, since the Bragg angle for the adder gratings must be so large that the grating period, and consequently, its angular acceptance range, is very small. This makes placement of these gratings and the associated lenses critical, requiring a placement

* By "mutually incoherent" we mean that no *stationary* interference pattern can result from superposition of the beams. Thus, it is in principle possible to use a single source with each coefficient frequency shifted sufficiently to average out the phase variations. This would, however, place a limit on the operation speed of the device.

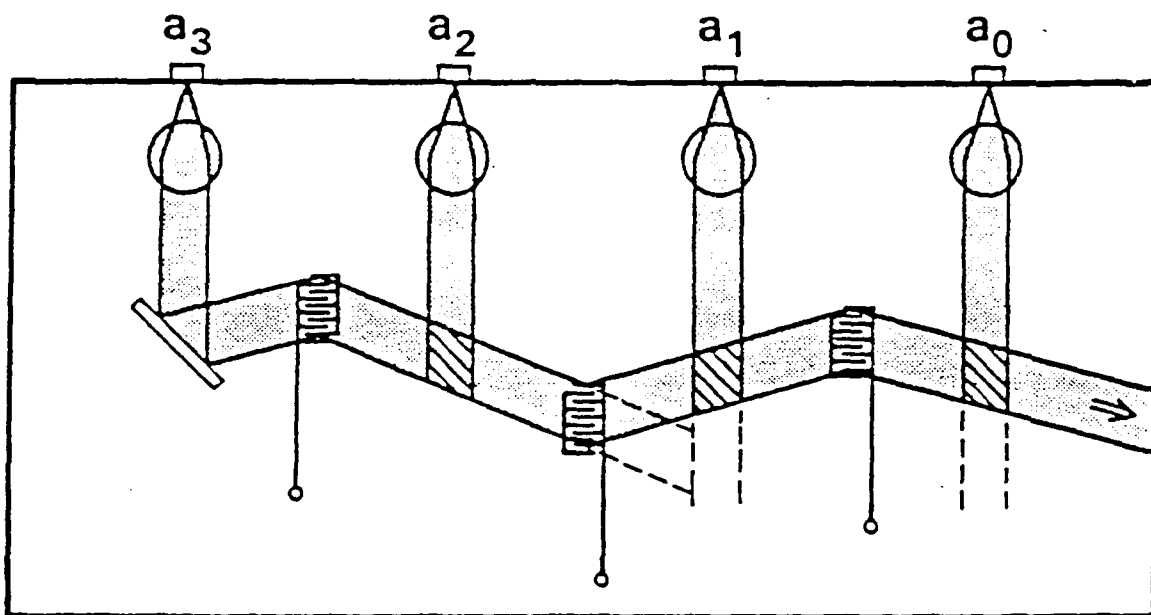


Figure 1. Schematic of original processor concept, using holographic surface gratings for adders and electrooptic overlap gratings for multipliers.

accuracy far beyond the current precision of integrated-optic fabrication. In addition, surface gratings are difficult to adjust in diffraction efficiency; the discussions in reference 2 show that extensive adjustments of both adder and multiplier gratings would be necessary in a practical device. It was therefore decided to look for architectures that would allow opening the angle at which the coefficients are introduced, thereby reducing the Bragg angle and increasing the angular acceptance range. It was also decided to see if the adder periods could be reduced sufficiently to make electrooptic adder gratings practical, as these gratings are simple to adjust in efficiency.

The original concept also included electrooptic multiplier gratings of a kind that has come to be called "overlap" gratings (a borrowing from holography), because the grating exists only in the region of beam overlap. Electrooptic gratings are simple to adjust in efficiency, but the overlap form of grating has two disadvantages:

- (1) The placement of the electrodes in the overlap region is critical. There are N of these gratings required, so easing the required precision of their placement is of extreme importance.
- (2) Overlap gratings produce diffracted outputs that have non-uniform profiles³. This nonuniformity in profile affects subsequent diffraction by both adder and multiplier gratings. This is further complicated by the fact that the actual profile obtained depends on the efficiency of the grating.

Both of these problems are alleviated by using the simpler grating forms analyzed by Kogelnik⁴ (and sometimes called "Kogelnik" gratings). For transmission, these gratings ideally would contain an infinite number of periods and a finite grating depth (length of the finger overlap in electrooptic grating electrodes). In practice, we need only assure that the grating contain enough periods to completely span the overlap region of the beams. The two kinds of grating are illustrated in Figure 2. The total vertical extent of the Kogelnik grating must at least accommodate the emphasized extent of the output beam. For this kind of grating, if the input beam is approximately a uniform plane wave, then the output beam will also be approximately a uniform plane wave. The width of the output beam is

$$W' = W + 2d \sin(\theta_B) \quad (2)$$

Because θ_B will be small for electrooptic gratings, the increase in width will also be small. For LiNbO_3 of index about 2.2, $\lambda = 784 \mu\text{m}$ and $\Lambda = 5 \mu\text{m}$, $\theta_B \approx 36 \text{ mrad}$, so a grating with finger

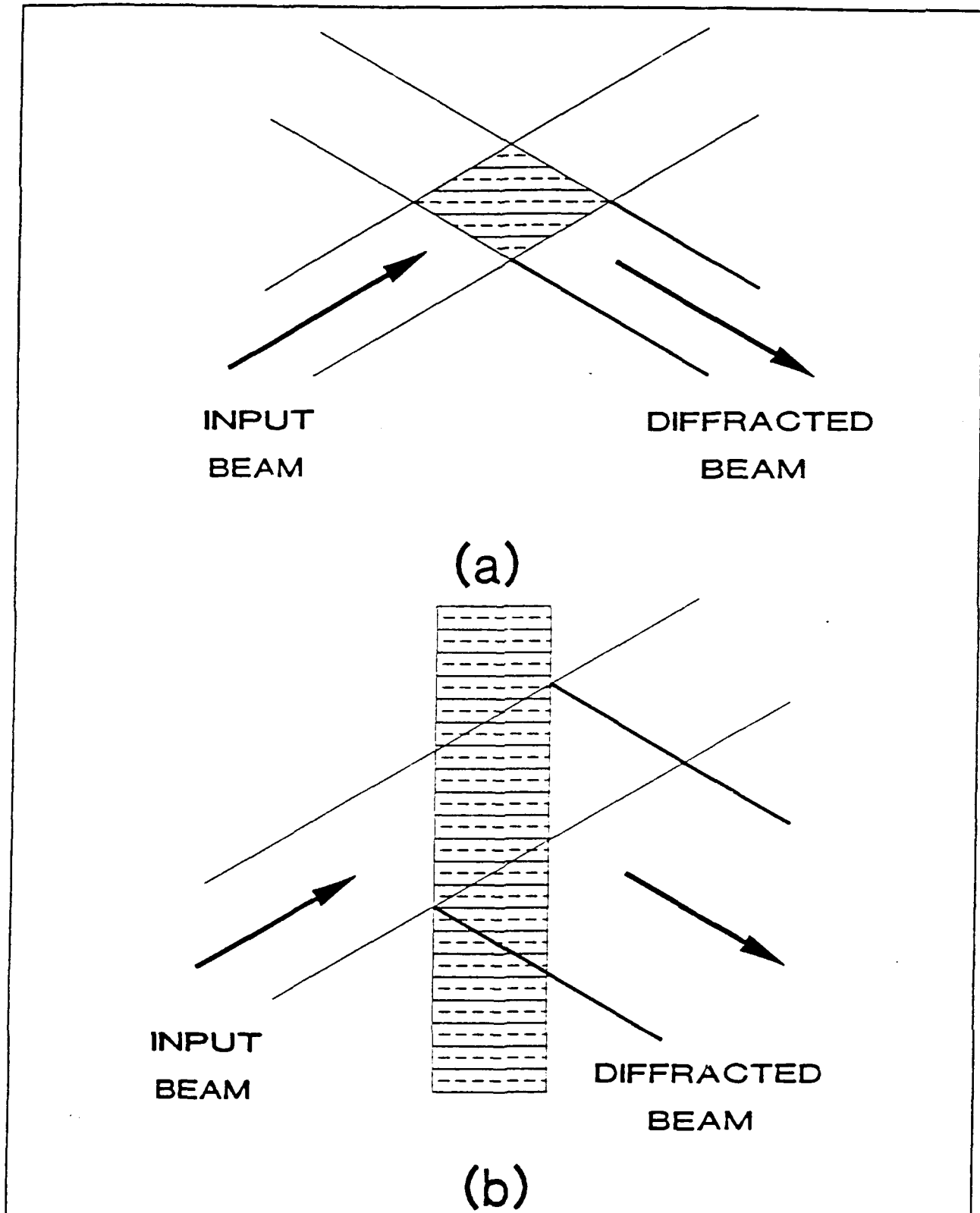


Figure 2. Illustration of grating types. (a) an overlap grating; (b) a Kogelnik grating. The output beam boundaries are emphasized.

overlap of $d = 1$ mm with a 1 mm input beam, the output beam will have its width increased by about $72 \mu\text{m}$. The required number of periods would then be

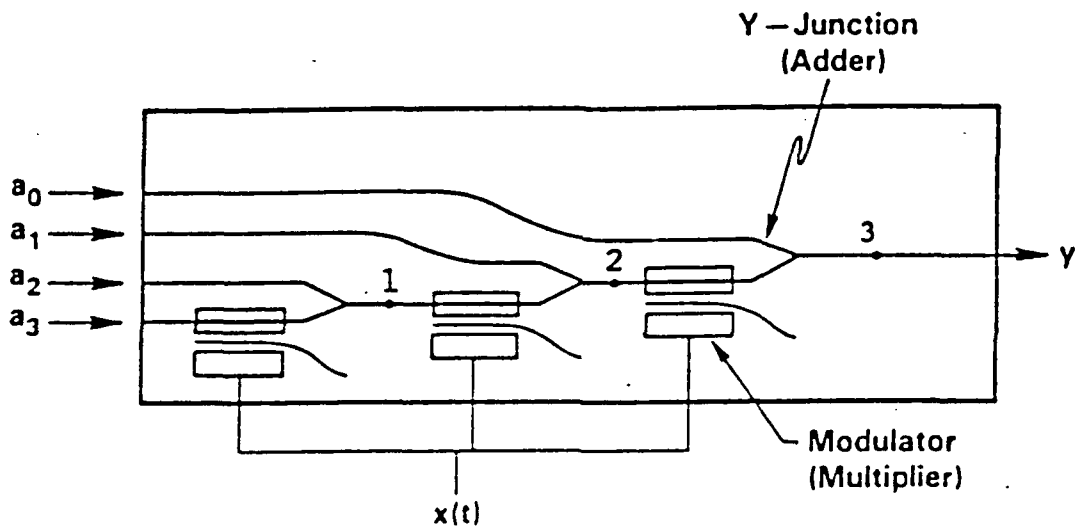
$$N_p = 1,072/5 \approx 215 \quad (3)$$

Because of the beam uniformity and noncritical alignment, these Kogelnik gratings were selected for the processor.

CHANNEL-GUIDE ALTERNATIVE LAYOUT

The planar-waveguide layout for the processor is not the only option available. In Figure 3 is illustrated one alternative, a channel-waveguide design that utilizes directional coupler modulators for switching light among the channels. Other kinds of switching are possible, but the directional coupler is the paradigm of this design. The channel device has a number of advantages, provided ideal operation can be achieved. First, channelized devices allow easy disposal of the light not coupled at a modulator; the light is simply ejected into the substrate and absorbed there. Second, there is less opportunity for light to scatter from channel guides into other parts of the processor, whereas in the planar guide, scattered light may cause noise. Finally, a channelized device need take little heed of the anisotropy of the LiNbO_3 crystal, whereas grating devices must be designed to accommodate the anisotropy if y- or x-cut crystals are used (for z-cut crystals, both TE and TM modes have effective indices that are independent of propagation direction).

The advantages of channelized architectures are not of an essential character, i.e., they are good to have, but not necessary to fabrication of a processor with good operating characteristics. On the other hand, one disadvantage of these devices is the critical fabrication required to obtain the desired range of coupling efficiencies. Directional couplers are very sensitive to errors in both the achieved effective index in the separated channels and the correct placement of the electrode structures. Another disadvantage is the length of the device required, not to achieve the coupling needed, but to bring the channels together and to separate them after the coupling. The final, and decisive, disadvantage is that the Battelle staff have extensive experience in fabrication of planar waveguides and with fabrication of electrode structures of small period upon them. There was a high-level of confidence in their ability to fabricate, successfully, a polynomial processor in a planar configuration. Their experience with channel guides was significantly less extensive. Our confidence in both our ability to design and their ability to fabricate a successful channelized processor was much lower. The planar design was therefore chosen.



$$I_1 \propto a_3 x + a_2$$

$$I_2 \propto (a_3 x + a_2)x + a_1$$

$$I_3 \propto [(a_3 x + a_2)x + a_1]x + a_0 = y$$

Figure 3. Schematic of a channelized version of the processor, using directional coupler modulators for light switching.

OVERALL SYSTEM CONSIDERATIONS

In addition to the design of the modulators and the beam-splitters, we must also consider the characteristics of the lenses and the light sources and the constraints which they place upon the remainder of the system before selecting a final design. This discussion is unified by concentrating attention upon the divergence of the guided beams and then establishing relationships among the various components in terms of this divergence.

Diffraction Limit

The fundamental constraint upon beam diffraction is given by

$$\Theta_{\text{diff}} = (\lambda_0/n_{\text{eff}})/w \quad (3)$$

where

λ_0 = free-space laser wavelength

n_{eff} = effective index of the guided light

w = minimum width of the guided beam.

For Sharp laser diodes, $\lambda_0 = 0.78 \mu\text{m}$. We can approximate the mode index as the material index for LNO which is in the range 2.2-2.3, depending upon the polarization. If we initially take $w = 1 \text{ mm}$, then

$$\Theta_{\text{diff}} \approx 0.35 \text{ mrad.}$$

GRATING CONSIDERATIONS

Basic Grating Equations

Grating diffraction in the Bragg regime is described by coupled-wave solutions derived by Kogelnik⁴. The appropriate solutions for our use are those for lossless transmission gratings. The efficiency is given generally by

$$\eta = \nu^2 \sin^2[\nu^2 + \xi^2]^{1/2} / [\nu^2 + \xi^2] \quad (4)$$

where ν and ξ are dimensionless parameters given by

$$\nu = \pi n_1 d / [\lambda_0 \cos(\theta_B)] \quad (5)$$

$$\xi = \vartheta d / 2 \cos(\theta) \quad (6)$$

and where the "dephasing" factor, ϑ , is

$$\vartheta = 2\pi[\sin(\theta) - \sin(\theta_B)]/\Lambda \quad (7)$$

Bragg Regime Diffraction Criteria.

The equations of the last paragraph *describe* diffraction in the Bragg regime, but leave unspecified any criterion for Bragg-regime diffraction. This is provided by the parameter ρ , called the Nath parameter and given by

$$\rho = (\lambda_0/\Lambda)^2/(n_0 n_1) \quad (8)$$

where λ_0 is the optical wavelength in vacuum, Λ is the grating period, n_0 is the average refractive index in the grating region, and n_1 is the refractive index modulation depth that comprises the grating. In an integrated optic system, n_0 is the effective refractive index of the guided mode. Bragg operation is generally achieved if ρ is large; a practical choice is $\rho > 10$. It can be shown⁵ that the higher-order diffracted beams are reduced relative to the first-order beams by a factor of approximately ρ^2 . Hence, requiring $\rho \geq 10$ will guarantee less than about 1% in higher-order diffracted beams.

ρ does not depend directly upon the grating depth, d . However, the polynomial evaluator requires that the grating efficiencies be set at specific values, and the Bragg efficiency of a grating depends on the product of n_1 and d . This introduces a coupling among the choices for n_1 , d and ρ . We have at Bragg incidence, where $\xi = 0$,

$$\eta_B = \sin^2(\nu) \quad (9)$$

If the efficiency is specified, then we will have

$$\rho = \pi \lambda d / [\Lambda^2 n_0 \cos(\theta_B) \sin^{-1}(\sqrt{\eta_B})] \quad (10)$$

which now has an explicit dependence on d . For our application, λ , Λ , n_0 and, therefore, θ_B , are fixed by a variety of other considerations. Hence, to achieve $\rho \geq 10$ with a uniform d , we need to have

$$d \geq \rho [\Lambda^2 n_0 \cos(\theta_B) \sin^{-1}(\sqrt{\eta_{B,\max}})] / (\pi \lambda) \quad (11)$$

where $\eta_{B,\max}$ is the largest required diffraction efficiency. Choosing $\eta_{B,\max}$ to be 1 is a safe choice. For $\lambda = 784 \mu\text{m}$, $n_0 = 2.2$ and $\rho = 10$, we find (setting $\cos(\theta_B) \approx 1$) $d = 322 \mu\text{m}$ for $\Lambda = 6 \mu\text{m}$ and $d = 223 \mu\text{m}$ for $\Lambda = 5 \mu\text{m}$. It will generally be advisable to choose larger values than these to ensure more complete suppression of the higher-order diffracted beams.

Grating Requirements

To get an estimate of the utility of the diffraction limit as a design criterion, we assume that all of the gratings will be formed photolithographically and ask what the acceptance angle of

a typical grating will be. Gratings with period $\Lambda = 3.5 \mu\text{m}$ can be fabricated; however, there is some question as to the ability of the maskmaker to fabricate masks containing several $3.5 \mu\text{m}$ gratings and of our ability to replicate such masks. We therefore assume a design limit of $\Lambda = 5 \mu\text{m}$ (we will ultimately choose periods of about $5 \mu\text{m}$ and $6 \mu\text{m}$) and take the grating width (finger overlap), d , to be 1.0 mm . Using the expression

$$\Delta\theta = \Lambda/d, \quad (12)$$

we find that the acceptance angle is 5 mrad . This is much larger than the diffraction spreading of a 1 mm -wide beam (0.4 mrad). Consequently we can use narrower beams if necessary and we can design other elements to a 4 mrad tolerance without excessive grating loss. Further, we adopt 3 mrad as an initial estimate of the upper limit of the beam divergence which can be tolerated from any other source.

Since the modulators have to operate on several wavelengths simultaneously, we must also look at the effect that the wavelength variation among the lasers has upon the modulator operation. The range of wavelengths accepted by a thick grating is

$$\Delta\lambda = 2n_0(\Lambda^2/d)\cos\theta \quad (13)$$

Again using the values $\Lambda = 5 \mu\text{m}$ and $d = 1.0 \text{ mm}$ we find that

$$\Delta\lambda = 110 \text{ nm}. \quad (14)$$

Examination of Table I, page 17, shows that there should be no difficulty in selecting lasers with a wavelength variation much smaller than this value.

It is important to realize that the various grating parameters are not entirely at our disposal. In particular, the characteristics of the processor dictate what the diffraction efficiencies of the gratings must be. This places a restriction on the values of the grating parameters. The efficiency is determined by the parameter ν , which involves the grating depth, d , and the index modulation amplitude, n_1 . The electrooptic effect relates this modulation amplitude to the applied voltage (V), the grating period (Λ), and material parameters. The requirement that $\rho > 10$ gives us another relation constraining n_1 , λ_0 and Λ . When all these are combined and we choose $\eta_{\text{max}} = 1$, we obtain the relation

$$\rho = 0.709(d/\Lambda^2) > 10 \quad (15)$$

or, approximately,

$$d > 14.1\Lambda^2 \quad (16)$$

where we have used the material parameters of LiNbO_3 , the wavelength $\lambda_0 = 0.78 \mu\text{m}$, and have assumed that the Bragg angle of the grating is small, so $\cos(\Theta_B) \approx 1$. When the choices discussed earlier are used ($\Lambda \approx 6 \mu\text{m}$, $d \approx 1.0 \text{ mm}$), we find $\rho \approx 19.7$, a very acceptable value.

Laser Characteristics

Ten Sharp laser diodes, four of which will be used in the processor, were purchased. The relevant laser characteristics are listed in Table I along with the values of beam divergence parallel and perpendicular to the junction and the laser wavelength. The output of the diodes is linearly polarized with the E-vector parallel to the plane of the junction. To minimize coupling losses we orient the laser with the plane of the junction perpendicular to the plane of the waveguide, thus using the minimum divergence angle for coupling. This choice has two consequences.

1. The modes in the waveguide will be TM modes.

2. The device will be more compact since the larger of the two angles is the one which relates to the beam divergence in the waveguide.

The data in Table I have been ordered according to the values of Θ_{PERP} , which is the divergence angle of the light in the plane of the waveguide. The

minimum angular spread for four lasers is 0.18 degrees which is the spread for lasers numbered 175, 176, 180, and 174. This angular spread will result in a 1.4 mrad variation in the divergence angle in the waveguide, which is well within the range of acceptance angles of the gratings. The wavelength spread for these four lasers is 5 nm which is also well within the acceptable range. We will assume that we will always be able to obtain sets of lasers with a divergence angle variation of less than 0.20 degrees (in air) or 1.6 mrad in the waveguide, and with a wavelength variation of less than 5 nm.

Table I. Data for Sharp Laser Diodes

LD No.	λ (um)	Θ_{PAR} (Deg)	Θ_{PERP} (Deg)
172	0.893	11.07	33.60
173	0.781	10.39	32.91
174	0.783	10.52	35.80
175	0.783	10.65	32.96
176	0.783	11.48	36.06
177	0.783	11.25	35.00
178	0.782	11.21	34.86
179	0.777	10.16	32.10
180	0.778	10.78	33.06
181	0.781	11.19	32.88
182	0.782	10.06	33.87
183	0.782	11.44	34.77

Lens Characteristics

The beam divergence in the waveguide is the divergence in air divided by the mode index, or approximately 0.25 rad. To convert this diverging beam to a 1 mm-diameter collimated beam requires an $f/4$ lens.

We will now calculate the accuracy to which an $f/4$ lens must be fabricated to collimate a beam to within ± 3 mrad and will also investigate the collimation error which will result from the variation in the laser divergence. We refer to Figure 4 where:

f = design focal length

ϵ = combined error in lens focal length and position

ϕ = $1/2$ source divergence angle = 0.13 rad (in waveguide)

δ = shift of extremal ray at center of lens

α = departure from true collimation.

From Figure 4 it can be seen that

$$\tan \alpha = \delta/f = (\epsilon/f) \tan \phi. \quad (17)$$

The requirement that $\alpha < 3$ mrad means that (ϵ/f) must be less than 0.023 or that the combined fabrication errors must be less than 2.3%. We believe that it will be possible to fabricate lenses to this accuracy.

Equation (17) can also be used to calculate the effects of the spread in the laser divergence upon the degree of beam collimation. Differentiating with respect to ϕ we get

$$d\alpha = (\epsilon/f) \sec^2 \phi \sec^{-2} \alpha d\phi \quad (18)$$

or

$$d\alpha \approx \epsilon/f d\phi. \quad (19)$$

If we assume a 2% fabrication error, then $\epsilon/f = 0.02$, and we see that a 0.36 degree spread in the laser divergences will result in a 0.008 degree error in the beam divergence. This is well within tolerable limits. The variation in laser divergence angle can therefore be ignored.

Substrate Orientation

There are several factors which can be considered in selecting the substrate orientation and the orientation of the pipeline upon the substrate. Among these are utilization of the maximum electrooptic coefficient, minimization of optical damage, and the operating requirements of the various integrated optical components. The most stringent requirement at this stage is set by the lenses. There are two types of lens being considered for the final version of the processor, an As_2S_3 Luneberg lens and a TIPE (titanium indiffused proton exchanged) mode

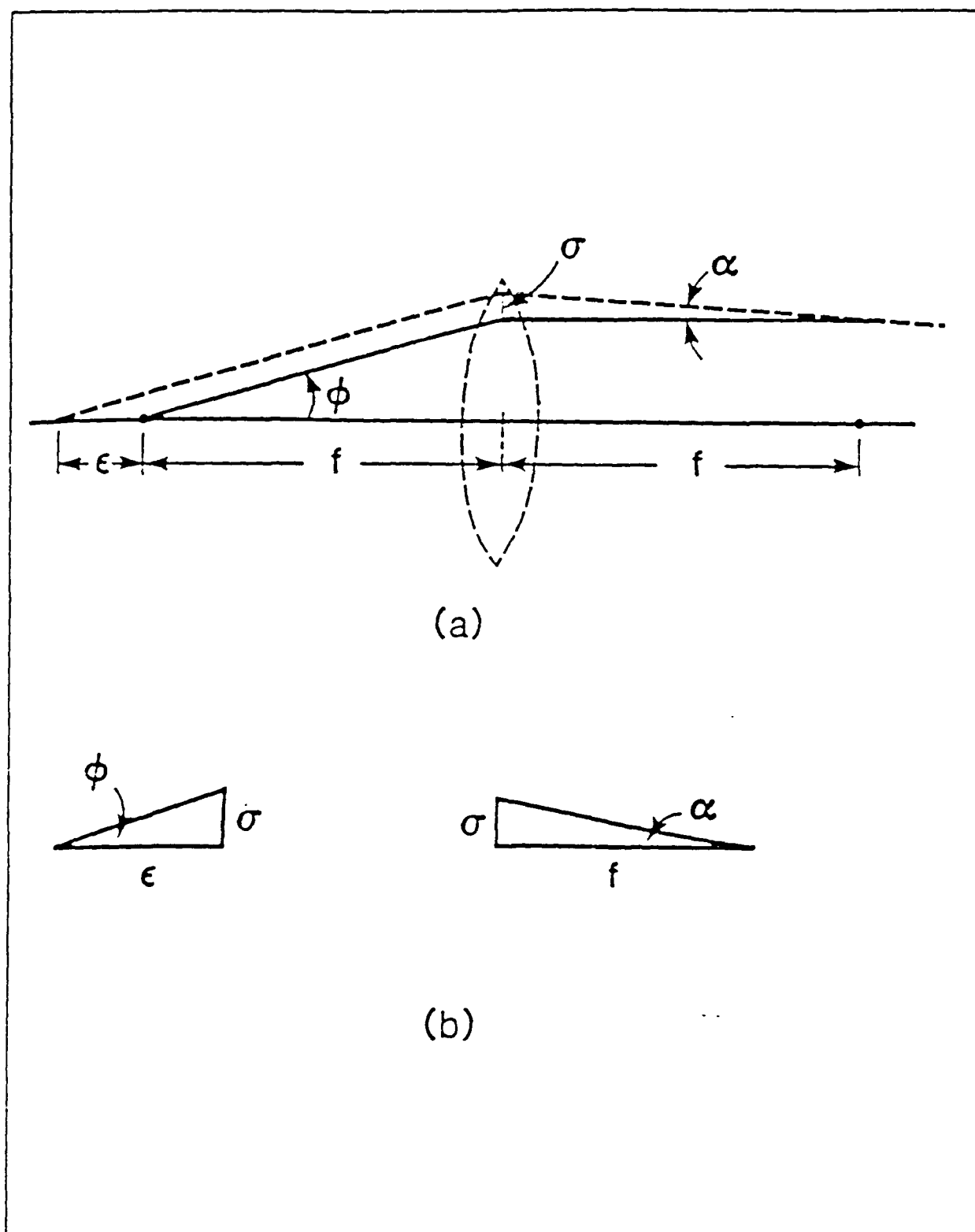


Figure 4. (a) Geometry used to calculate the collimation error associated with a lens fabrication error ϵ ; (b) details showing angular relations.

-index lens. The proton-exchange process alters only the extraordinary index of refraction of the lithium niobate. Since the laser characteristics dictate TM polarization, the TIPE process further restricts us to z-cut crystals. In order to preserve the option of using TIPE lenses, z-cut substrates were used for this design.

A summary of the choices resulting from these system considerations is displayed in Table II.

Table II. Summary of System Choices

Substrate orientation: z-cut
Diffraction spread for 1 mm beam: 0.35 mrad (in waveguide)
Beam spread design limit: 3 mrad (in waveguide; based on grating requirements)
Waveguide modes: TM (extraordinary)
Available laser wavelength: $782 \pm 2.5 \text{ nm}$
Available laser beam divergence: 33.24 ± 0.10 degrees ($0.58 \pm .002 \text{ rad}$) (in air)
Available divergence range: $\pm 1.0 \text{ mrad}$ (in waveguide)
Allowable laser wavelength spread: $\pm 79 \text{ nm}$ (based upon grating requirements)
Allowable lens fabrication tolerance: 2.3%

DESIGN CONSIDERATIONS

DESIGN LAYOUT OPTIONS

Two basic options for the device layout were examined. These options both represent a departure from the layout of Figure 1 in that the coefficient beams are introduced from the left end of the substrate in order to open the beam angles and reduce the Bragg angle of the "adder" gratings. This reduction of Bragg angles makes the fabrication tolerances for the placement and focal length of the lenses less stringent, bringing them to within the current technology for both Luneburg lenses and for the favored "TIPE" lenses.

A second departure from Figure 1 is the use of simple, unslanted gratings for both multipliers and adders. This reflects our decision to use Kogelnik-style gratings for multipliers instead of overlap gratings. This choice also allows more compact design.

The following is intended as a brief description of these options, will appear in the next report. The design options are as follows:

Option 1:

Coefficients are entered from above the system axis (SA) at a simple polished face of the substrate and impinge on equally-spaced "adder" grating elements, where they are incorporated into the signal stream. This is illustrated in Figure 5. In this layout, the separation of the sources along the sloped input edge must be large enough to accommodate their coupling into the waveguide. Alternate adder gratings are tilted

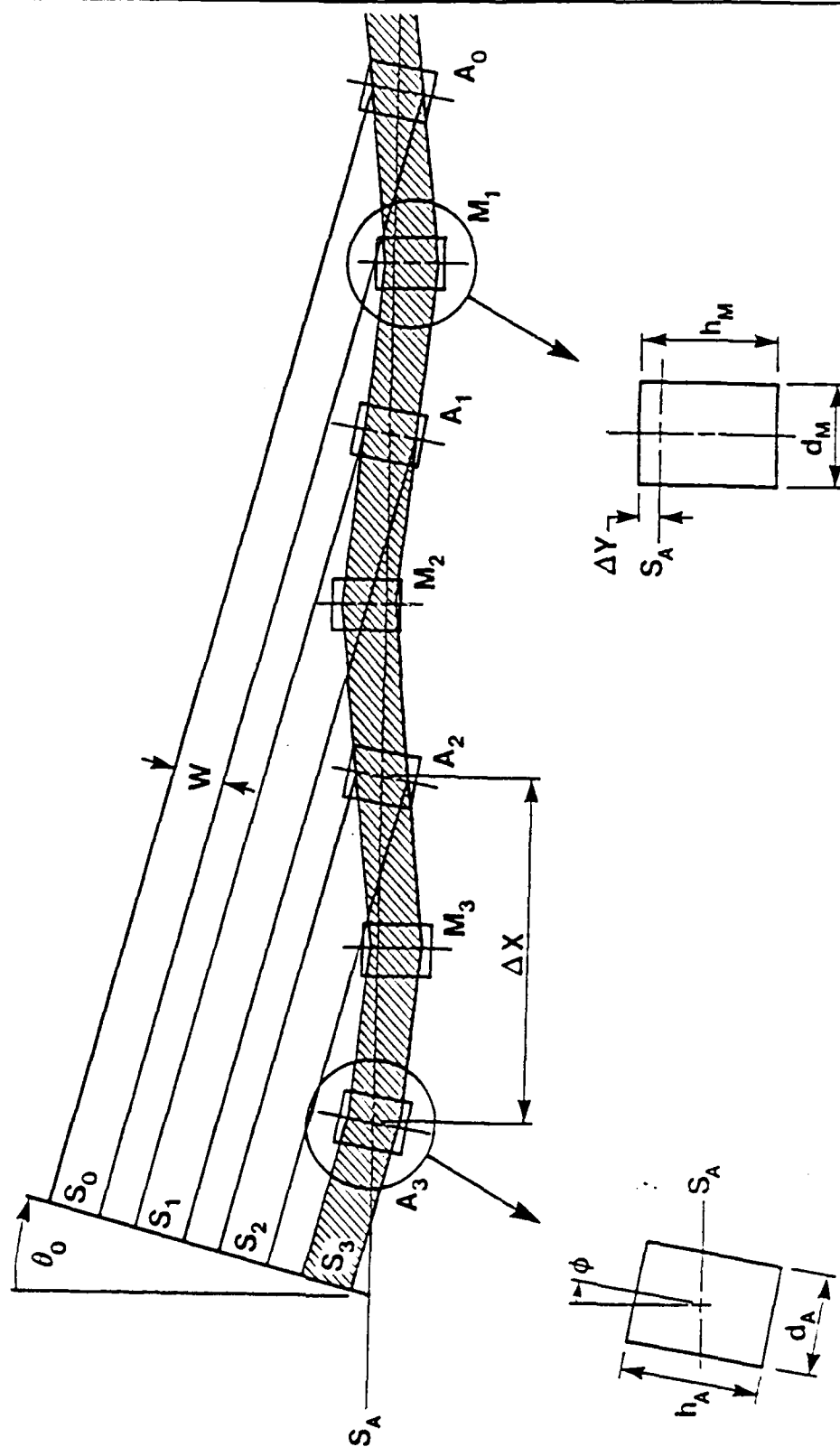


Figure 5. Schematic illustration of Option 1 for the processor layout.

relative to the SA, with slightly differing tilt angles, and have different periods. The multiplier gratings in both options are upright and have a single period.

Option 2:

Coefficients are entered alternately from above or below the SA at a compound polished face of the substrate and impinge on equally-spaced "adder" grating elements. This is illustrated in ?. In this option, separation of the sources to accommodate coupling is easier, since alternate sources are "missing" on both input slopes. Alternate adder gratings are tilted, alternately, relative to the normal to the SA, but all have the same period.

Multiplier gratings, as in Option 1, are upright and have a single period.

Two critical questions needed to be answered about these options:

- "How closely can the adder and multiplier gratings be spaced?"
- "How small can the Bragg angles be made?"

Close spacing of the elements has a direct impact on the device length, limited by crystal availability to about 75 mm, maximum. One immediate consequence of this consideration was the abandonment of the use of so-called "overlap" gratings — gratings that just fill the diamond-shaped overlap region where two beams intersect. These gratings tend to be wasteful of crystal area when electrooptic gratings (as in the multiplier gratings) are involved, because of the small Bragg angles. Furthermore, the alignment problem is considerably aggravated if these gratings are used. Where small Bragg angles are contemplated, simple, unslanted gratings are more desirable, since the depth (length of the fringes or overlap of the electrode fingers) of these gratings is controllable independently of other device design parameters.

Small Bragg angles for the gratings generally result in less stringent alignment and manufacturing precision for lenses and because achievement of very small Bragg angles would allow use of all-electrooptic gratings, the grating alignment would be accomplished by the maskmaker. Once a suitable mask were available, all device samples would be correctly aligned in fabrication.

OPTION 1 ANGULAR RELATIONS

In Option 1, all coefficient beams are introduced from above the SA. The signal beam zig-zags above and below the axis at angles θ_{BM} (Bragg angle for Multiplier gratings). As a result, alternate adder gratings (Bragg angle: θ_{BA}) have different periods (since they must accomplish different deflections of the coefficient beams to introduce them into the signal stream. They are also tilted at different angles with respect to the normal to the SA.

The odd-numbered adder gratings deflect the coefficient beams into a downward leg of the zig-zag signal path, as illustrated in Figure 7. We see that

$$\theta_0 = 2\theta_{BA}^{(ODD)} + \theta_{BM} \quad (20)$$

Figure 6. Schematic Illustration of Option 2 for the processor layout.

and that these adders are tilted by the angle

$$\begin{aligned}\phi_A^{(ODD)} &= [\theta_0 + \theta_{BM}]/2 \\ &= \theta_{BA} + \theta_{BM}\end{aligned}\quad (21)$$

with respect to the normal to the SA.

The even-numbered adder gratings deflect the coefficient beams into an upward leg of the zig-zag signal path, as illustrated in Figure 8. Here,

$$\theta_0 = 2\theta_{BA}^{(EVEN)} - \theta_{BM} \quad (22)$$

and the adders are tilted at the angle

$$\begin{aligned}\phi_A^{(EVEN)} &= [\theta_0 - \theta_{BM}]/2 \\ &= \theta_{BA} - \theta_{BM}\end{aligned}\quad (23)$$

with respect to the normal to the SA.

OPTION 2 ANGULAR RELATIONS

The angular relations for Option 2 are similar to those of Option 1, but are slightly simpler. The coefficient beams are introduced alternately from above (odd-numbered beams) and from below (even-numbered beams) the SA, while the signal beam zig-zags across the axis, as in Option 1. The alternating directions for the coefficient beams, combined with the zig-zag path of the signal beam, lead to adder gratings that all having the same period and that alternately tilt to the right and to the left by a constant angular magnitude, relative to the normal to the SA.

There are two ways to arrange the adder gratings in this option: 1) both the signal beam and the coefficient beam are directed away from the SA; and 2) one beam is directed towards the SA and the other is directed away. Case 2) leads to a larger Bragg angle for the adders (smaller grating period).

Case 1 (Figure 7)

The relationship between θ_0 and the Bragg angles is

$$\theta_0 = 2\theta_{BA} + \theta_{BM} \quad (24)$$

Figure 8. Angular Relations for Option 1, Even Adders or Option 2, Case 2, Odd Adders (Reflect in SA for Even Adders).

(as for the odd-numbered adders in Option 1). The adder gratings are tilted relative to the normal to the SA by the angle

$$\begin{aligned}\phi_A &= [\theta_0 + \theta_{BM}]/2 \\ &= \theta_{BA} + \theta_{BM}\end{aligned}\tag{25}$$

with the odd-numbered gratings tilted CW and the even-numbered ones tilted CCW.

Case 2 (Figure 8)

θ_0 and the Bragg angles now have the connection

$$\theta_0 = 2\theta_{BA} - \theta_{BM}\tag{26}$$

and the tilt of the adder gratings is given by

$$\begin{aligned}\phi_A &= [\theta_0 - \theta_{BM}]/2 \\ &= \theta_{BA} - \theta_{BM}\end{aligned}\tag{27}$$

We see at once that if the multiplier and adder gratings have the same Bragg angle, then the adder gratings are not tilted. This has a significant advantage from the viewpoint of photolithographic mask fabrication because the electrode mask would not involve angles. However, in this configuration, any stray beam striking any grating would do so at Bragg incidence. Hence, one would require complete separation of beams between stages, thus lengthening the device. Small Bragg angles (as required in all-electrooptic devices) then lead to longer devices.

These angular relations connect the grating periods and the zig-zag path of the signal beam, for both options, to the single angle, θ_0 , between the coefficient beams and the SA. Once θ_0 is chosen, the angular relationships restrict the range of periods that can be used. The restrictions on periods that occur because of photolithographic limitations then impose further restrictions. In the final case discussed, of course, θ_0 is just equal to the common Bragg angle of the gratings, and no further choices are available.

DESIGN OF THE PHOTOMASK

The critical design task of the project is the design of the photomask. The design choices were made in light of the discussions above, and were based upon the selection of Layout Option 2 with "Kogelnik"-style electrooptic gratings used throughout. The design was also based upon the use of a TM mode, propagating in a z-cut crystal of maximum dimension about 75 mm. This mode and crystal cut reflects the future need to butt couple laser diodes to the waveguide and to leave open the choice of TIPE lenses for future designs.

SELECTION OF GRATING PARAMETERS

Selection of Grating Periods.

The grating periods were chosen under three constraints:

- (1) There is a photolithographic limit to reliable fabrication of these gratings. We set the minimum period at 5 μm .
- (2) The period of the multiplier grating has a strong effect on the overall length of the device; the effect of the adder-grating period is of second order, and may be neglected.
- (3) The maskmakers informed us that the tilt angles of the gratings could be specified only to the nearest 0.1° , and that the finger widths should be specified only to the nearest 0.1 μm . Further, the gratings were to be made by repetition of the pattern for a single "finger", and the positioning accuracy during this assembly of a grating reticle was given as 0.01 μm .

The first of these merely constrains the range of periods available, and is easily accommodated. The second item is a result of the constraints imposed by proper handling of the undiffracted beams. This is discussed under the heading "Management of Undiffracted Beams" in the section "System Considerations", presented earlier. There, it was found that the spacing between sources, S (recall that S is defined relative to Option 1) must satisfy

$$S \geq (2R+1)(W + h)/4 \quad (28)$$

where $R = \theta_A/\theta_M$, W is the beam width, and h is the larger of h_M and h_A . The device size is approximately $4S/\cos(\psi)$, where ψ is the angle made by the source line and the system axis; $\psi = \pi/2 - (2\theta_A + \theta_M)$. Inserting this into the constraint on S gives

$$L_{\text{total}} \geq (W + h)/\theta_M \quad (29)$$

which depends only on θ_M . If we set $\Lambda_M = 5 \mu\text{m}$, $W = 1 \text{ mm}$ and $h = 1.2 \text{ mm}$ (the actual final design values), we find for $\lambda = 784 \text{ nm}$ & $n = 2.2$ the device length of 61.7 mm, close to the final value of 58.4 mm, the difference being attributed to the weak dependence on θ_A .

From this, it is apparent that small multiplier periods are desirable, but that the adder period can be relaxed somewhat, to allow for more reliable fabrication.

The third constraint, imposed by the maskmaker, means that we cannot use arbitrary periods for the gratings. If we take $\Lambda = 5 \mu\text{m}$ for the multiplier gratings and $\Lambda = 6 \mu\text{m}$ for the adder gratings as nominal design targets, then the finger widths for the multipliers will be $1.25 \mu\text{m}$. This can be adjusted to 1.2 or $1.3 \mu\text{m}$; then the spaces between the fingers can be adjusted in the opposite way (to 1.3 or $1.2 \mu\text{m}$) to preserve the period. The restriction on the positioning accuracy of "fingers" to assemble a grating reticle restricts the period specification to only the nearest $0.02 \mu\text{m}$, because one finger and one space makes only half of a period.

The restriction on angular positioning means that the tilt of an adder, $\phi = \theta_{BM} + \theta_{BA}$, can be specified only to 0.1° . Since it was desired to place a fiducial mark along the source line, at angle $\psi = 2\theta_{BA} + \theta_{BM}$, this angle, too, could only be specified to 0.1° , resulting in the overall requirement that each Bragg angle should be specified individually only to this accuracy.

These maskmaker's restrictions were accommodated by constructing a table of grating periods, rounded to the nearest $0.1 \mu\text{m}$, for Bragg angles in the range 1.7° to 2.1° in increments of 0.1° . Then, starting from the nominally-desired Bragg angle, the corresponding period was found in the table, and the actual Bragg angle was re-calculated for comparison to the nominal one. Agreement to within a few milli-degrees was required and obtained for all designs. The final design parameters selected are displayed in Table III

MANAGEMENT OF UNDIFFRACTED BEAMS

We can now proceed to a design based on the use of electrooptic gratings throughout and on the overall system analysis presented earlier in this report. Our first task is to derive relations that will allow us to trace the coefficient and signal beams, as well as the undiffracted beams resulting from them, through the whole device. Since the devices of order one, two and three will be based upon the same basic design, we work with the largest proposed device, which has four adders and three multipliers. Using Option 2, Case 1, we see that

$$\theta_0 = 2\theta_{BA} + \theta_{BM} \quad (30)$$

We define the following quantities (we take the origin of coordinates to lie at the left end of the SA, at the edge of the crystal):

X_{Ai} = x-coordinate (along SA) of center of adder # i

X_{Mi} = x-coordinate (along SA) of center of multiplier #i

Table III. Final Device Parameters

General Data:

Operating Wavelength	0.783 μm
Crystal Cut	z-cut
Mode and Propagation Direction	TM ₁ x-propagating
Substrate Index	2.1784
Surface Index	2.1834
Superstrate Index (Buffer Layer)	1.5
Effective Index of Guided Mode	2.1799
Electrooptic Coefficient	$3.05 \times 10^{-5} \mu\text{m}/\text{V}$
Fill Factor	0.3

Multiplier Grating Data:

Bragg Angle	2.0 deg
Period	5.14 μm
Depth (Finger Overlap)	1.00 mm
Height	1.20 mm
Nath parameter @100% d.e. ($\approx 16.75 \text{ V}$)	27

Adder Grating Data:

Bragg Angle	1.7 deg
Period	6.06 μm
Depth (Finger Overlap)	1.00 mm
Height	1.20 mm
Nath parameter @ 100 % d.e. ($\approx 19.65 \text{ V}$)	20

Grating Placement Data:

Spacing between adder gratings on S.A.	15.76 mm
Center of first adder on SA (A_3)	10.628 mm
Center of second adder on SA (A_2)	26.389 mm
Center of third adder on SA (A_1)	42.150 mm
Center of fourth adder on SA (A_0)	57.911 mm
Tilt angle of adder gratings	$\pm 3.70 \text{ deg}$
Vertical offset of multiplier gratings	$\pm 0.551 \text{ mm}$
Center of first multiplier grating (M_3)	18.509 mm
Center of second multiplier grating (M_2)	34.270 mm
Center of third multiplier grating (M_1)	50.031 mm

Source Spacing Data:

Position of first source (S_3)	1.00 mm
Spacing between sources	2.96 mm

Y_{Mi} = y-coordinate (from SA) of center of multiplier $\neq 1$

S = spacing between coefficient beams that would obtain for Option 1.

S_i = position of i-th coefficient source, measured from origin along perpendicular to the coefficient beams;

$$S_1 = S_3 + S; S_2 = -S; S_0 = -2S \quad (31)$$

h_A = height of an adder grating (number of periods times the length of a period)

h_M = height of a multiplier grating (number of periods times the length of a period)

w = the width of the optical beam

We then have that $\Delta X = S/\sin(\theta_0)$ is the distance between the adder grating centers, and that

$$X_{Ai} = X_{A3} + (3-i)\Delta X, i=0,1,2,3 \quad (32)$$

with

$$X_{A3} = S_3/\sin(\theta_0) \quad (33)$$

Also,

$$X_{Mi} = (X_{Ai} + X_{Ai-1})/2 \quad (34)$$

$$Y_{Mi} = \mp \Delta X \sin(\theta_{BM})/2 \quad (35)$$

The sign of y is positive for even i , negative for odd i .

Continuing along these analytical lines, we display the equations of the centerlines of the various beams. These are not strictly necessary for our present purposes, since we are here concerned mainly with deriving geometrical constraints to minimize re-diffraction of stray beams. However, they will be useful for later calculations.

Coefficient Beams:

$$C_i: \quad y = (-1)^i [x - x_{Ai}] \tan(\theta_0) \quad (36)$$

$$(x \geq S_i \sin(\theta_0), i=1,2,3,4)$$

Undiffracted Coefficient Beams (indicated by a prime, ')

$$C'_i: \text{ Same equations as above, with } x \geq x_{Ai} \quad (37)$$

Signal Beam:

$$y - Y_{M3} = + |x - X_{M3}| \tan(\theta_{BM}) \quad \text{if } X_{A3} \leq x \leq X_{M2} \quad (38)$$

$$y - Y_{M2} = - |x - X_{M2}| \tan(\theta_{BM}) \quad \text{if } X_{M3} \leq x \leq X_{M1} \quad (39)$$

$$y - Y_{M1} = + |x - X_{M1}| \tan(\theta_{BM}) \quad \text{if } x \geq X_{M1} \quad (40)$$

Undiffracted Signal Beams:

$$y - Y_{Mi} = (-1)^i [x - X_{Mi}] \tan(\theta_{BM}) \quad \text{with } x \geq X_{Mi}, i=1,2,3 \quad (41)$$

The allowable x -ranges for the signal beams actually overlap; this has no real significance.

These equations describe the centerline of the beams. To obtain the upper (lower) limits of the beams, we simply add (subtract) half of the beam width (w) from the Y_{Mi} or the Y_{Ai} , as

appropriate. We can now systematically examine each beam as it progresses through the device and determine which gratings it impinges upon, the angle of incidence and the fraction of the beam width involved.

Re-diffraction of Stray Beams

The coefficient input beams, upon encountering the adder gratings, are only partly diffracted into the signal beam. Similarly, the signal beam, upon encountering a multiplier grating, is only partly diffracted as the signal beam changes direction. The undiffracted beams resulting from these encounters represent potential problems, as they may continue on to encounter later gratings of the system and be partially diffracted or scattered into the signal beam. Such accidental re-diffractions or scatterings of the "waste" light energy must be eliminated to avoid erroneous results. In this section, we examine this possibility and ways to avoid it.

There are only four directions in which a waste beam may progress, namely, $\pm\theta_0$ for the coefficient beams and $\pm\theta_{BM}$ for the signal beam. We denote these beams as follows:

C_+ is a coefficient beam remnant, progressing at angle $+\theta_0$;

C_- is a coefficient beam remnant, progressing at angle $-\theta_0$;

S_+ is a signal beam remnant, progressing at angle $+\theta_{BM}$;

S_- is a signal beam remnant, progressing at angle $-\theta_{BM}$.

Adder Gratings

We recall that for Option 2, Case 1, the [even/odd] adder gratings are tilted by $\pm(\theta_{BA} + \theta_{BM})$ relative to the normal to the SA; and that $\theta_0 = 2\theta_{BA} + \theta_{BM}$. Thus, stray beams impinging on an adder grating strikes it at the following angles of incidence:

$$C': \pm (2\theta_{BA} + \theta_{BM}) \pm (\theta_{BA} + \theta_{BM}) \quad (42)$$

$$S': \pm \theta_{BM} \pm (\theta_{BA} + \theta_{BM}) \quad (43)$$

For both sets, the combinations having opposite choices of signs lead to incidence at $\pm\theta_{BA}$. These correspond to a C' beam from an odd (even)-numbered adder impinging upon another odd (even)-numbered adder or to a S' beam from an odd (even)-numbered multiplier impinging upon an odd (even)-numbered adder grating. In both cases, there is an intervening even (odd)

numbered adder grating which may intercept the stray beam, but cannot diffract it efficiently*, because the angles are so large. To understand this, consider the case where the adder and multiplier gratings have the same period. In that case, the like-sign combinations give $5\theta_B$ and $3\theta_B$ angles of incidence. These beams are deflected weakly by $-2\theta_B$ (to good approximation); so, they emerge at approximately at $3\theta_B$ and θ_B , respectively--they do not change sense from "up" to "down". Hence, the direct, first-order diffraction orders are weak and not in the signal direction. Second-order diffraction terms would emerge, after deflection by $-4\theta_B$, at $+\theta_B$ and $-\theta_B$, respectively, exactly in the signal beam. This points up the importance of having the Nath parameter, ρ , as large as feasible. A value of 20 reduces the second-order beams by a factor of about 400; since these orders must compete for light with the first-order terms, having $\rho=20$ effectively removes them from consideration.

Multiplier Gratings

For the multiplier gratings, the undiffracted beams always impinge on other multiplier gratings at the Bragg angle, so *the undiffracted light from a multiplier grating must clear the following multiplier gratings entirely*. Undiffracted light from adder gratings cannot strike multipliers at Bragg incidence.

DESIGN CONSTRAINTS: LAYOUT

It is a simple geometrical exercise to calculate the dimensional restrictions that must be imposed to avoid re-diffraction of waste beams. When all-electrooptic gratings are used, Bragg angles will be small, and small-angle approximations can be used, making the results especially simple. The procedures follow below. These calculations neglect the thickness (d) of the gratings. The "exact" results would be slightly modified from those given below if d were accounted for, but the small-angle results would be the same.

Adder Gratings

Stray light from odd (even)-numbered adder gratings that impinges on another odd (even)-numbered adder grating must propagate a total distance of $2\Delta X$ at an angle of θ_0 , with

$$\Delta X = S/\sin(\theta_0) \quad (44)$$

Hence, to clear the second grating, the beam width, grating height and source spacing must be related by

* There could be some random scattering from the grating if there is no buffer layer between the guide and the electrodes; very little of this light should be scattered directly into the signal beam.

$$2\Delta X \tan(\theta_0) > \{W/\cos(\theta_0) + h_A/\cos\theta_{BA} + \theta_{BM}\}/2 \quad (45)$$

or, for small angles

$$S > (W + h_A)/4 \quad (46)$$

This will be easily reached for realistic values of W and h_A .

Stray light from an odd (even)-numbered multiplier grating that impinges on an odd (even)-numbered adder grating must traverse $3\Delta/2$ at the angle θ_{BM} . We must also remember that the multiplier gratings are offset from the SA by $\pm\Delta X \tan(\theta_{BM})/2$. Hence, we must have

$$\Delta X \tan(\theta_{BM})/2 + 3\Delta X \tan(\theta_{BM})/2 > \{h_A + W/\cos(\theta_{BM})\}/2 \quad (47)$$

or, for small angles,

$$S > (2R+1)(W + h_A)/4 \quad (48)$$

where

$$R \equiv \theta_{BA}/\theta_{BM} \quad (49)$$

is the Bragg-angle ratio, which will be nearly 1. This restriction is a little more severe than the one found above, but is easily met also.

Multiplier Gratings

The requirement that the multiplier gratings have no stray signal beams impinging on them is

$$2\Delta X \tan(\theta_{BM}) > \{h_M + W/\cos(\theta_{BM})\}/2 \quad (50)$$

or, for small angles,

$$S > (2R+1)(W + h_M)/4, \quad (51)$$

similar to the second constraint for the adder gratings, with h_A replaced by h_M . The factor of 2 on the left-hand side of this equation results from the offset of the multiplier gratings.

We can conclude that meeting the geometrical constraints for best stray beam management will not be difficult.

FABRICATION ISSUES

PRELIMINARY FABRICATION STUDIES

As a preliminary step to fabrication, a small amount of time was spent photolithographically generating diffraction gratings on lithium niobate waveguides using arsenic trisulfide (As_2S_3), aluminum, and chrome. The gratings were experimentally examined to determine the diffraction efficiency for the various samples. This information was intended to assist in determining the material requirements for the diffraction gratings within the processor. The following discussion provides a brief description of the grating design parameters.

Grating Evaluation Experiments

Six Ti:LiNbO_3 waveguides were fabricated on Y-cut and Z-cut samples using the following trial fabrication parameters:

Titanium Thickness:	280 Angstroms
Diffusion Temperature:	1020 C
Diffusion Time:	5 hours
Out-diffusion Suppression:	0.5 SCCM FLOWING O_2

In addition to the flowing O_2 , the out-diffusion of lithium was further suppressed by placing two boats of lithium niobate powder within the tube furnace in proximity with the samples during diffusion.

After the planar waveguides were completed the surfaces were coated with the grating materials. Table IV lists the grating materials applied to the LiNbO_3 waveguides.

An existing photolithographic mask was used to generate the diffraction gratings in the surface materials. The mask consists of 0.875 micron lines separated by 0.875 micron spaces. The lines were one millimeter long and the grating aperture was 7 millimeters in length. Standard photolithographic techniques were used to generate two grating patterns on each waveguide, with

Table IV. Fixed Surface Grating Sample Parameters

Guide	Crystal Cut	Grating Material
-	-	-
PP-Y-1	Y-CUT	1500 Å As_2S_3
PP-Y-2	Y-CUT	1000 Å ALUMINUM
PP-Y-3	Y-CUT	1000 Å CHROME
PP-Y-4	Y-CUT	1000 Å CHROME
ZZ-6	Z-CUT	1000 Å ALUMINUM
ZY-6	Z-CUT	1500 Å As_2S_3

the gratings set perpendicular to one another. This allows the measurement of diffraction efficiency of light propagating approximately parallel to each of two crystal axes.

The diffraction efficiency of each grating was measured using a HeNe laser ($\lambda = 632.8$ nm) with both TE and TM polarization. Table V summarizes the results of the diffraction

efficiency experiments for 5 of the 6 samples. The sixth sample, which contains a chrome grating was not tested.

Table V. Results of Diffraction Grating Experiments

Waveguide	Grating Material	Polarization	Prop. Dir.	Diffr. Eff.	Refr. Index
PP-Y-1	As ₂ S ₃	TE	X	94.6 %	n _e
		TM	X	60.3 %	n _o
		TE	Z	65.2 %	n _o
ZY-6	As ₂ S ₃	TM	Z	29.7 %	n _o
		TE	X	41.8 %	n _o
		TM	X	27.1 %	n _e
		TE	Y	8.1 %	n _o
PP-Y-2	Aluminum	TM	Y	50.0 %	n _e
		TE	Z	0.1 %	n _o
		TM	Z	36.3 %	n _o
		TE	X	28.3 %	n _e
ZZ-6	Aluminum	TM	X	47.8 %	n _o
		TE	X	1.9 %	n _o
		TM	X	42.7 %	n _e
		TE	Y	1.9 %	n _o
PP-Y-3	CHROME	TM	Y	38.5 %	n _o
		TE	X	1.3 %	n _o
		TM	X	9.1 %	n _o
		TE	Z	2.3 %	n _o
		TM	Z	13.6 %	n _o

Processor Waveguide Fabrication

All of the waveguides fabricated for the diffraction grating experiments had a single mode at $\lambda = 840$ nm. Although they were never tested with $\lambda = 783$ nm (the design wavelength for processor) it is believed that they would have two modes.

To determine the proper recipe to yield single mode guides for Z-cut LiNbO₃ at $\lambda = 783$ nm a number of test waveguides were fabricated. The following trial recipe was used to make the waveguides; the variation from the previous recipe should be noted.

CRYSTAL CUT:	Z
TITANIUM THICKNESS:	250 Å
DIFFUSION TEMPERATURE:	1000 C
DIFFUSION TIME:	5 hours
OUT-DIFFUSION SUPPRESSION:	4 SCCM flowing O ₂

The waveguides were tested using a HeNe laser ($\lambda = 632.8$ nm). Two of the waveguides had TiO₂ residue on the surface and were highly scattering. The third waveguide, fabricated

separately, has low scattering and was a good waveguide. Figure 9 shows the mode plots of the waveguide at $\lambda = 632.8$ nm for both TE and TM polarizations.

From Table V one can see that the As_2S_3 grating was the most efficient, as one might expect. However, it is significant that many of the metal gratings efficiently diffract the light and that with most of the metal gratings the TM polarized light was diffracted with higher efficiency than the TE polarized light, even though there was no buffer layer between the metal grating and the waveguides. It was therefore concluded that the TM modes interact more strongly with the metal electrodes than the TE modes, so, a buffer layer will certainly be needed for TM operation. Such a layer might also be needed for TE operation.

Modulator Fabrication and Evaluation

In this section we outline the parameters and methods for fabricating the electrooptic modulators using the pipelined polynomial processor mask. We then report the results of the fundamental modulator evaluations.

Modulator Fabrication

Several planar integrated-optic waveguides were fabricated on 1 inch by 1 inch, Z-cut lithium niobate samples using the following (final) fabrication parameters.

Titanium Thickness	250Å
Diffusion Time	6 Hours
Diffusion Temperature	1000°C

The out diffusion of lithium was suppressed by flowing O_2 over the samples and placing two boats of lithium niobate powder next to the samples during diffusion. The waveguides were evaluated to determine the number of modes with HeNe light. Most had one dominant mode for both TE and TM light and a weak higher order mode. The samples were polished for 3 hours. This reduced the surface roughness and suppressed the higher-order modes.

The electrode structure was delineated onto the waveguide surface using image reversal techniques, since the photomask was a dark-field mask. The 10-step procedure used is listed in Table VI

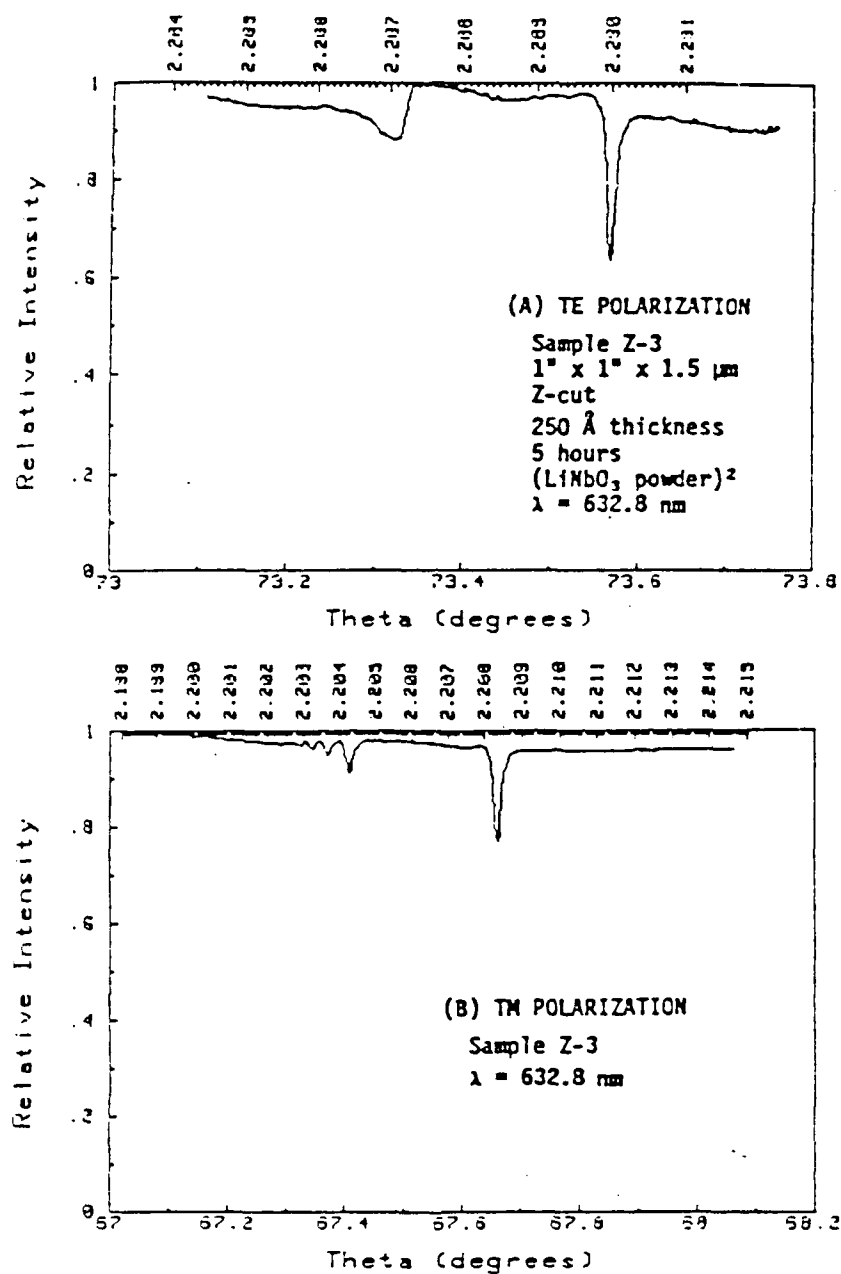


Figure 9. Mode Plots for Z-cut Lithium Niobate Waveguide ($\lambda=632.8 \text{ nm}$; Ti thickness = 250 Å; diffusion time = 5 hours; diffusion temperature = 1000°C).

Sample Characterization

One sample, Z-6, was evaluated using both TE and TM polarization using a HeNe laser beam propagating along the y axis. Prism coupling was used to couple the light into the waveguide. A small prism was placed between the two gratings to couple the diffracted and undiffracted light out of the waveguide.

As expected, TM modes were highly absorbed by the chrome electrodes. The TE polarized light propagated with little attenuation.

Figure 10 shows the diffraction efficiency as a function of voltage for both TM and TE polarized light. For the TM polarized light a maximum diffraction efficiency of about 80% was measured at 12 volts, with a diffracted power of 0.0266 μ watts. For TE polarized light, the measured maximum diffraction efficiency was 96.5%, with a diffracted power of 0.845 μ watts.

Significant "charging effects" were found with the Z-cut crystal. 40 volts was applied to the electrodes for a few minutes, then quickly the voltage was quickly set to zero. A residual 30% diffraction efficiency was then found. This residual was reduced to zero only by the application of 6 volts in the reverse direction. This charging effect is observed only with z-cut crystals, and is a disadvantage to using this cut.

Table VI. Electrode Delineation Procedure

1. Clean waveguides and mask.
2. Evaporate 1000Å chrome onto waveguide surface.
3. Spin on POS photoresist with 1% (by weight) Imidazole at 4000 rpm for 40 sec.
4. Bake photoresist coated sample at 85°C for 30 minutes.
5. Expose sample through dark-field mask for 5 seconds using heavy finger pressure to achieve intimate contact.
6. Bake sample at 100°C for 30 minutes.
7. Flood expose sample for 10 seconds.
8. Develop photoresist in P-2 developer for 8 seconds.
9. Etch chrome with GF Smith Etchant for 75 seconds.
10. Strip photoresist with acetone.

PROCESSOR EVALUATION

Initial evaluation of the processor components were made in X- and Y-cut crystals for convenience and to eliminate the DC charging effects and the attenuation of TM polarized light observed with Z-cut crystals.

Portions of the polylithium polyniobate processor were fabricated on several Y-cut and X-cut lithium niobate samples containing good planar optical waveguides. The mode indices for the six waveguide samples were measured using a computer-controlled apparatus. Three laser sources were used in the evaluation: a HeNe laser ($\lambda = 632.8$ nm), a Sharp laser diode ($\lambda = 784$ nm) and a

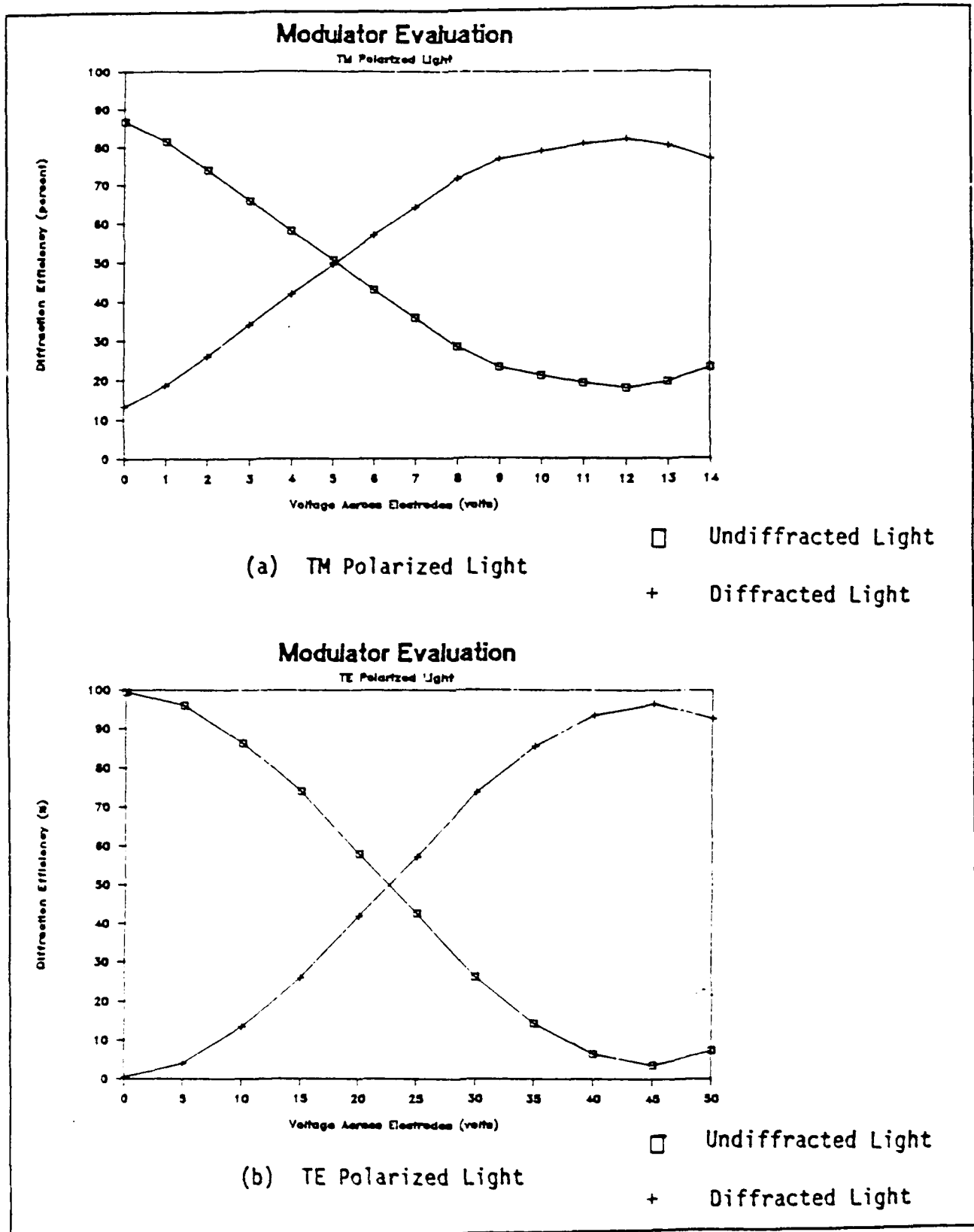


Figure 10. Diffraction efficiency plots for modulator gratings.

Hitachi laser diode ($\lambda = 840$ nm). The measured mode indices for the waveguide samples are summarized in Table VII.

The diffraction efficiency of several electrooptic gratings were measured as a function of

Table VII. Measured Mode Indices for Planar Optical Waveguides

Sample	Wavelength	<-----Refractive Index----->		
		Bulk	TE ₀	TE ₁
PPY-1	632.8nm	2.2024	2.2060	2.2027
	784nm	2.1772	2.1798	2.1774
PPY-4	632.8nm		2.2064	2.2029
	784nm	2.1770	2.1809	2.1772
	840nm	2.1716	2.1743	2.2172
AX-2	784nm	2.1780	2.1782	
AX-3	784nm	2.1778	2.1784	
221-Y	784nm	2.1776	2.180	2.1781
241-Y	784nm	2.1778	2.1783	

applied voltage. Figure 11(a) and Figure 11(b) show the diffraction efficiency curves for an adder grating at wavelengths of 632.8 nm and 784 nm, respectively.

All of the sample processors contained adder grating A1 and multiplier grating M2, which were used in all of the initial experiments. The Bragg angle of both the multiplier and adder gratings was measured and an apparent angular misalignment between the adjacent gratings was found and quantified. The Bragg angles were determined by precisely measuring the angular alignment of the lithium niobate substrate when maximum Bragg diffraction of the electrooptic modulators occurred with light propagating from below the grating ($-\theta_B$) and with light propagating from above the grating ($+\theta_B$).^{*} These precise angular measurements along with the mode indices were used to determine the Bragg angle using the equation:

$$\theta_B = (\theta_1 - \theta_2)/(2n) \quad (52)$$

* Strictly speaking, these measurements determined the deflection produced by the gratings; the actual Bragg angles, measured relative to the grating fingers, deviates slightly from half of the deflection angle because of anisotropic diffraction in the x- or y- cut crystals. This effect will not occur in z-cut crystals. This is discussed more at the end of the report.

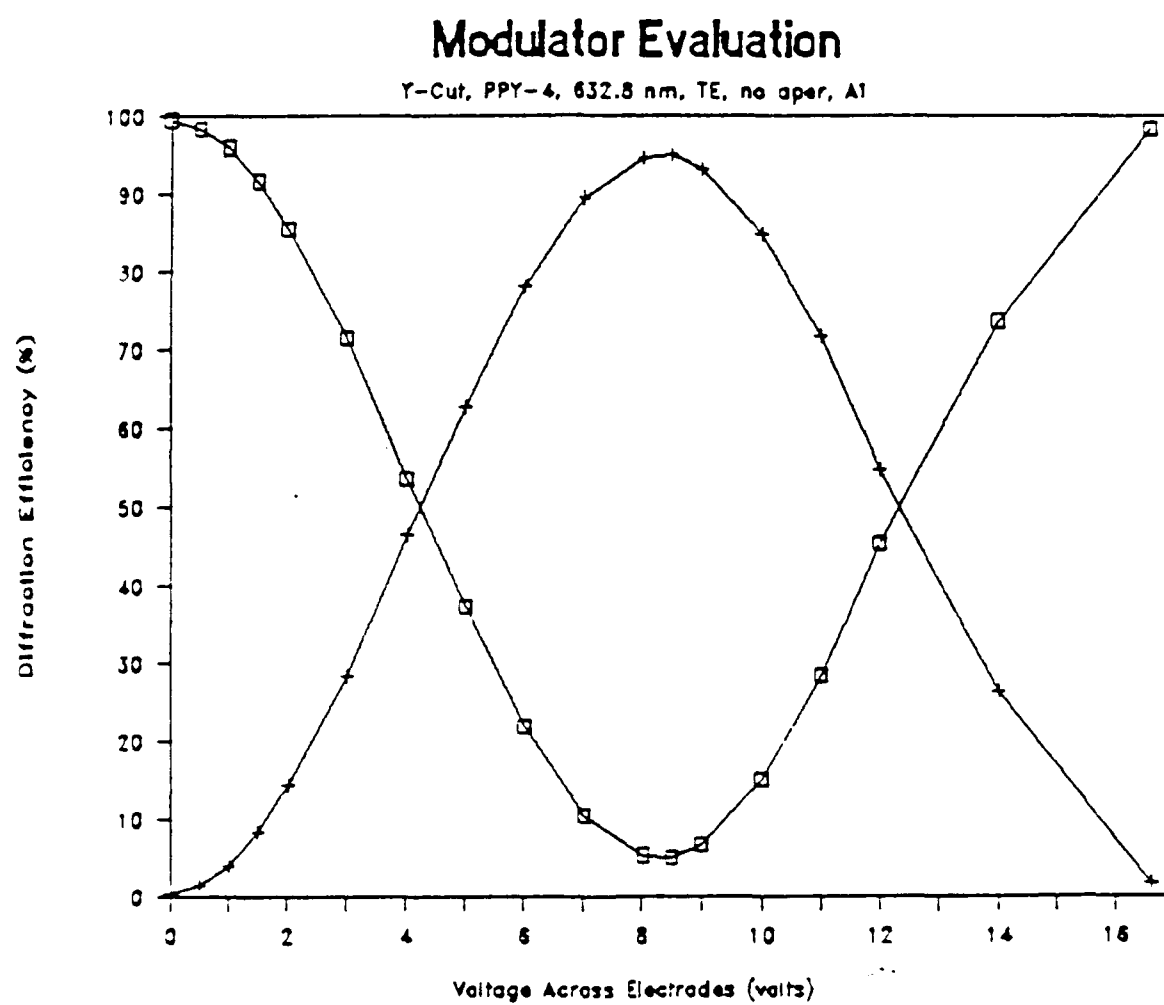


Figure 11. Diffraction efficiency of an adder grating at a wavelength of 632.8 nm

where Θ_1 and Θ_2 are the angular positions of the substrates when maximum Bragg diffraction occurs, and n is the mode index of the planar optical waveguide.

The angular misalignment between adjacent electrooptic gratings was determined by orienting the light so that it is incident on the adder grating at the positive Bragg angle (Θ_{BA}) and incident angle the multiplier at the negative Bragg angle ($-\Theta_{BM}$), as shown schematically in Figure 12. If the two adjacent gratings were perfectly aligned and their voltages were adjusted for less than 100% diffraction efficiency, then we would expect to see an undiffracted beam parallel to the incident beam, a diffracted spot from the adder grating on one side of the undiffracted spot and a diffracted spot from the multiplier grating on the other side of the undiffracted spot.

The angular misalignment was determined by measuring the angular orientation of the lithium niobate substrate when maximum Bragg diffraction occurred for the adder grating and the multiplier grating. These angular measurements along with the mode indices are used to determine the angular misalignment using the expression

$$\Theta_{MA} = (\Theta_{1A} - \Theta_{1M})/n \quad (53)$$

where Θ_{1A} and Θ_{1M} are the measured orientations of the substrate for maximum Bragg diffraction by the adder and multiplier, respectively, and n is the mode index of the planar optical waveguide. The measured Bragg angles and angular misalignments are summarized in Table VIII.

It is interesting to note that the measured Bragg angles at the design wavelength ($\lambda = 784$ nm) are very close to the design values (within the measurement capability) but the angular misalignment at that wavelength is significant (this misalignment limited the double diffraction efficiency to less than 20%). The photomask angles were measured under a microscope with a precision rotation stage and found that the angles were as specified to the measurement accuracy. Extrapolation of the angular misalignment data at wavelengths of 632.8 nm and 784 nm led to the estimate that the angular misalignment would be zero at a wavelength of 840 nm. This was then verified on two samples (PPY-1 and PPY-4) using the Hitachi laser diode. The explanation for this apparent misalignment is given in the next section.

ANISOTROPIC DIFFRACTION

The initial evaluation studies made on adjacent gratings for the processor were made, as indicated earlier, on samples fabricated upon x- and y- cut crystals, using TE-polarized light. The device was designed, however, for z-cut crystals and TM-polarized light. Because LiNbO_3 is a uniaxial crystal, light of only two (orthogonal) polarizations, called ordinary and extraordinary

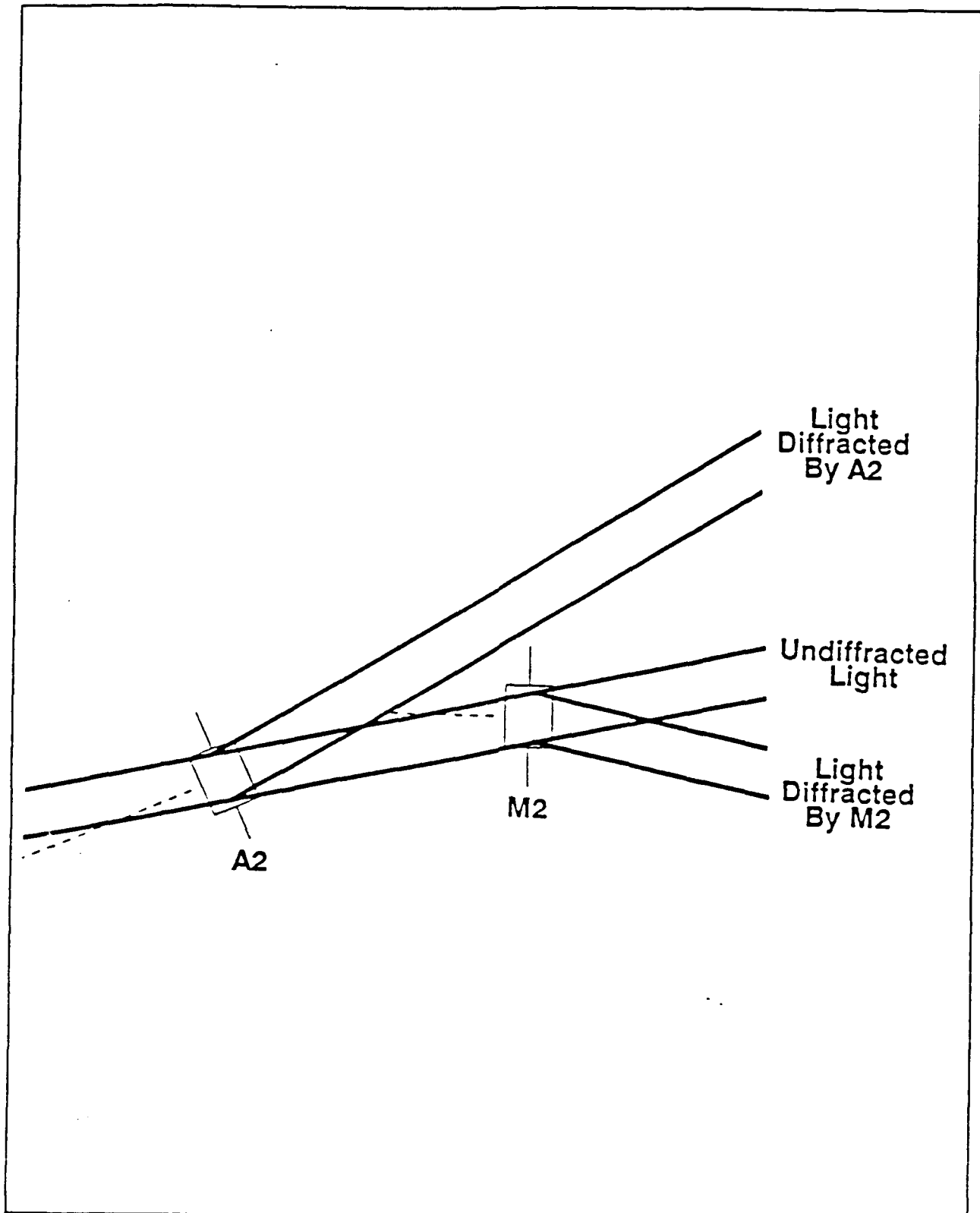


Figure 12. Schematic representation of light propagating through two adjacent electrooptic modulators. Perfect angular alignment will result in simultaneous diffraction by gratings A_2 and M_2 .

Table VIII. Measured Bragg Angles and Angular Misalignments

Sample	Wavelength (nm)	Mode Index	<----Bragg Angles---->		Angular Misalignment (deg)
			Adder (deg)	Multiplier (deg)	
PPY-1	632.8	2.206	1.36	1.59	1.13
	784	2.1798	1.72	2.03	0.31
	840	2.1743 ^a	1.84	2.17	0
PPY-4	632.8	2.2064	1.36	1.61	1.10
	784	2.1809			0.31
	840	2.1743	1.84	2.17	0
AX-2	784	2.1782	1.68	2.03	0.23
AX-3	784	2.1784	1.72	2.15	0.34
221-Y	784	2.18	1.76	2.03	0.31
241-Y	784	2.1783	1.76	2.03	0.31

^aThe mode index of PPY-1 at 840 nm was not measured. The value for PPY-4 was used

polarizations, can propagate in the material. Light entering the crystal polarized in other directions excites a superposition of these two eigen-polarizations.

In waveguides fabricated upon an x- or a y-cut crystal (crystal surface perpendicular to the x or y crystallographic direction, resp.), light polarized in the waveguide plane corresponds to the extraordinary polarization, and its effective refractive index varies with propagation direction within the plane of the guide, in an elliptical fashion. For light that propagates along the z-axis, the extraordinary index is equal to the maximum extraordinary index, n_o , while light propagating along the x axis sees the minimum extraordinary index, n_e . The conditions for Bragg diffraction are altered by this direction dependence of the effective modal index of refraction. This alteration is small if the propagation directions are close to the crystalline axes (either x or y), as is the case under consideration. However, this small change is highly significant for gratings having a low ratio of period to grating thickness, because this ratio governs the sensitivity of the diffraction efficiency to deviations from Bragg incidence. For our processor gratings, this ratio is in the range .006 for the adder gratings to .005 for the multiplier gratings.

Fortunately, the change in Bragg angle due to anisotropic diffraction can be calculated exactly. The relevant formulas are as follows:

$$\tan(\Theta_B) = [y_o n_o^2 + mR] / [m y_o n_o^2 - R] \quad (54)$$

where

$$y_o^2 = F(1 - F[n_g \sin(\phi) / 2n_o n_o]^2) \quad (55)$$

$$R = F n_g \sin(\phi) / 2 \quad (56)$$

$$n_g = K/k \quad (57)$$

$$F = n_o^2 + m^2 n_g^2 \quad (58)$$

$$m = \cot(\phi) \quad (59)$$

In these equations, n_o and n_g are the maximum and minimum values of extraordinary index for LiNbO_3 , mentioned earlier; ϕ is the deviation of the grating vector, \underline{K} , from the y-axis; K is the magnitude of the grating vector,

$$K = 2\pi/\Lambda; \quad (60)$$

Λ is the grating period; n_g is the grating "index", or normalized grating vector,

$$n_g = K/k, \quad k = 2\pi/\lambda \quad (61)$$

and λ is the vacuum wavelength of the light. Using this formula and the design parameters for the device, we find that the Bragg angle for the adder grating is 5.676° , against the design value for z-cut crystals and TM light of 5.40° . The difference, 0.28° , is very close to the measured value of 0.31° (for $\lambda = 0.784 \mu\text{m}$).

The multiplier gratings are unslanted, i.e., \underline{K} points along a crystalline axis, $\phi = 0$, and m becomes infinite. It is easier to treat this case directly; the resultant formula is

$$\tan(\Theta_B) = (n_g/n_o)/[1-(n_g/n_o)^2]^{1/2}. \quad (62)$$

The calculated deviation from the designed Bragg angle of 2.0° is less than 0.001° .

We conclude from this that the apparent misalignment of the gratings is simply the result of anisotropic diffraction, and not any error in the mask manufacture. When z-cut crystals were used, this effect was not present.

FABRICATION ON Z-CUT SUBSTRATES

Two z-cut devices each with three electrooptic gratings and one z-cut device on a 3-inch long substrate with all seven electrooptic gratings were fabricated. Table IX summarizes the fabrication process.

EVALUATION OF Z-CUT PROCESSORS

Table IX. Fabrication Parameters for Pipelined Polynomial Processor

<u>Substrate:</u>	
Material	Lithium Niobate
Crystal Cut	Z-Cut
<u>Waveguide:</u> (Ti Indiffused LiNbO ₃)	
Ti Thickness	220Å
Diffusion Temperature	1000°C
Diffusion Time	5 Hours
Diffusion Suppression	50 SCCM O ₂ + Powdered LiNbO ₃
<u>Buffer Layer:</u>	
Material	7059 Glass
Thickness	1500Å
Anneal Temperature	600°C
Anneal Time	≈ 70 Hours
<u>Electrodes:</u>	
Material	Aluminum
Thickness	1000Å

After successfully fabricating several z-cut device samples the diffraction efficiency was evaluated as a function of electrode voltage and the angular alignment and X-Y position of the electrodes. It was found that the voltages required for maximum diffraction are very large, which is expected because of the low dielectric constant of the buffer layer. Voltages between 45 and 55 volts are required to achieve maximum diffraction efficiency (>95%).

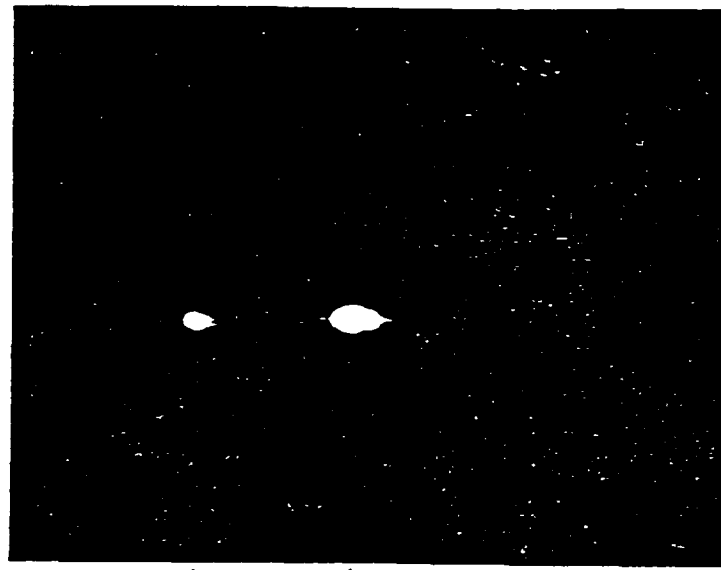
The angular alignment between adjacent gratings was found to be correct in these samples, verifying that anisotropic diffraction was responsible for the apparent misalignment. More than 95% of the incident light was diffracted with an adder grating (A_2) and more than 95% of this singly-diffracted light was diffracted through a second electrooptic grating.

The possibility of X-Y position misalignment between adjacent electrooptic gratings was investigated by simultaneously illuminating both an adder grating (A_2) and a multiplier grating (M_2). The input laser light from a Sharp laser diode ($\lambda = 784$ nm) was oriented so that it was incident on the adder grating at the positive Bragg angle ($+\theta_{BA}$) and incident on the multiplier grating at the negative Bragg angle ($-\theta_{BM}$), as shown schematically in Figure 12. When a 2-mm-diameter beam was used to illuminate the grating some stray undiffracted light from the edge of A_2 did reach M_2 and was subsequently diffracted. When the aperture was reduced to 1 mm this stray light did not reach M_2 , leading to the (incorrect) belief that the gratings were positioned correctly. Later studies revealed that the multiplier gratings were, because of a design error,

placed just twice as far from the SA as they should be, leading to a useful aperture of 0.5 mm instead of the designed 1.0 mm.

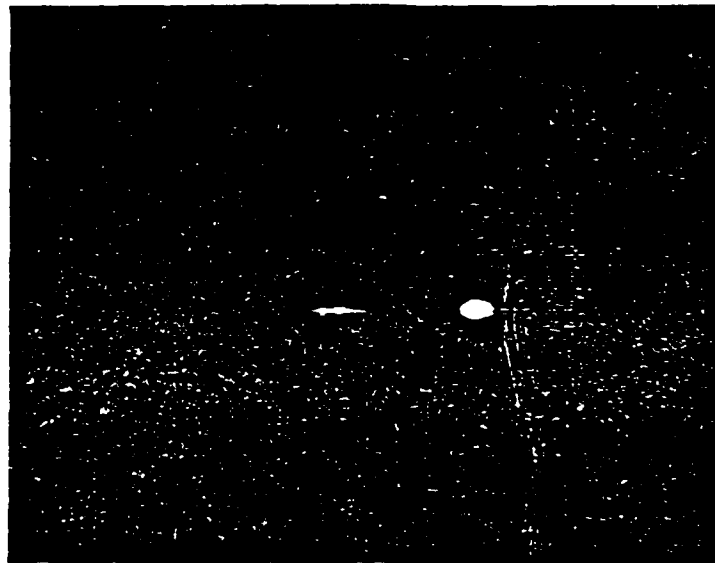
Figure 13(a) and Figure 13(b) show the resulting output spots for two test cases. In case 1 the laser beam was oriented as shown schematically in Figure 12, and 15 volts (expect a low diffraction efficiency) were applied to M_2 and 0 volts (zero diffraction efficiency) to A_2 . The resulting photograph, shown in Figure 13(a), shows the undiffracted light (zero-order beam) and a small amount of light diffracted by M_2 .

Figure 13(b) shows the second case which is identical to case 1 (15 volts on M_2) except that 50 volts (expect high diffraction efficiency) are applied to A_2 . The photo shows very little light in the zero-order beam, and a bright spot representing the light diffracted by A_2 . Very little light made it to M_2 and, consequently, no detectable light was diffracted by M_2 .



M_2 0 A_1

(a)



M_2 0 A_1

(b)

Figure 13. Images of diffracted and undiffracted light from two adjacent modulators. (a) 0 V on A_1 , 15 V on M_2 ; (b) 50 V on A_1 , 15 V on M_2 .

IMPLEMENTATION OF SQUARE-ROOT PROCESSOR

INTRODUCTION

In this section, the generation of second-order polynomial $x^2 - N = 0$ is discussed. The motivation for implementing this simple device is that its positive zero is the square root of N . The rapid evaluation of square roots has applications in radar processing; this application represents the simplest use of a polynomial processor to perform a non-trivial operation.

The device was implemented using sample #PPZ-4. This sample contained three gratings, the first and third of which were driven in parallel to represent the value of x , while the center grating acted as a mirror. Light from a laser diode (LD #175) was prism coupled into the sample such that it was incident on the first grating at the Bragg angle. Light was prism coupled out of the waveguide and detected using a power meter. The output of the power meter was fed into an op-amp circuit as the non-inverted input while a d.c. voltage was used as the inverted input, representing the constant, N . The output of the op-amp circuit was viewed on an oscilloscope where the data could be graphically interpreted. The functionality of the device was evaluated by varying the d.c. input and observing the oscilloscope trace.

EXPERIMENTAL SETUP

The waveguide sample that we used was designed as having two adder gratings separated by a multiplier grating. In the experiment, the roles of these gratings were reversed, with the two adder gratings functioning as multipliers, and the single multiplier as the mirror. Figure 14 shows the layout of the sample where M_1 and M_2 denote the first and second multiplier gratings (tilted adder grating in fact); A_1 denotes the mirror grating (an untilted multiplier grating) and S_1 denotes the input laser beam. Light is coupled into the sample from the left at the Bragg angle for M_1 . The diffracted light in the first order is

$$I_1 = I_i \sin^2(\alpha V)$$

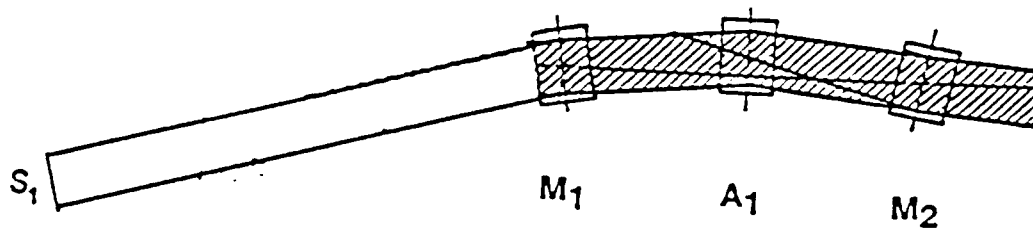


Figure 14. Spatial layout of PPZ-4 device. S_1 denotes the input laser beam, M_1 and M_2 denote the multiplier gratings, and A_1 denotes the adder grating.

where I_1 is the intensity of light in the first order diffracted beam, I_i is the intensity of the incident beam on the grating, α is a constant and V is the voltage applied to the grating. In order to achieve linear proportionality between the diffracted light and the applied voltage, the voltage applied to the first and third gratings was made artificially proportional to the arcsine of $x^{1/2}$ * and the voltage applied to the second (middle) grating was a constant d.c. value. Therefore, that,

$$I_1' = I_i \sin^2(\arcsin[x^{1/2}]) = I_i x$$

$$I_2' = I_1' \sin^2(C_1) = I_i a_1 x,$$

$$I_3' = I_2' \sin^2(\arcsin[x^{1/2}]) = I_i a_1 x^2.$$

where I_i' is the diffracted intensity from the i^{th} grating and I_i is the intensity incident on the first grating. a_1 is a constant, representing the coefficient "1", and x is a variable that we will ramp linearly.

The arcsine of $x^{1/2}$ voltage was generated by a programmable function generator (see Figure 15). The output of the function generator was then amplified by an audio amplifier to increase the voltage of the signal to the appropriate level to drive the multiplier gratings at their peak efficiency (~ 45 volts). To assure that the output from the amplifier was always a positive voltage, it was necessary to add a clamping circuit to the amplifier output. An unfortunate drawback of this design is the .7 volt drop that occurs across the diode in the clamping circuit which is significant to our output for small values of x . This drop (-.7 volts) can be seen in the lower left corner of Figure 15.

* The $\sin^{-1}(\sqrt{x})$ processing is needed because of the nonlinear response of the grating to applied voltage. In practice, one would be more likely to utilize the IO device directly, then remove the nonlinearity in post processing.

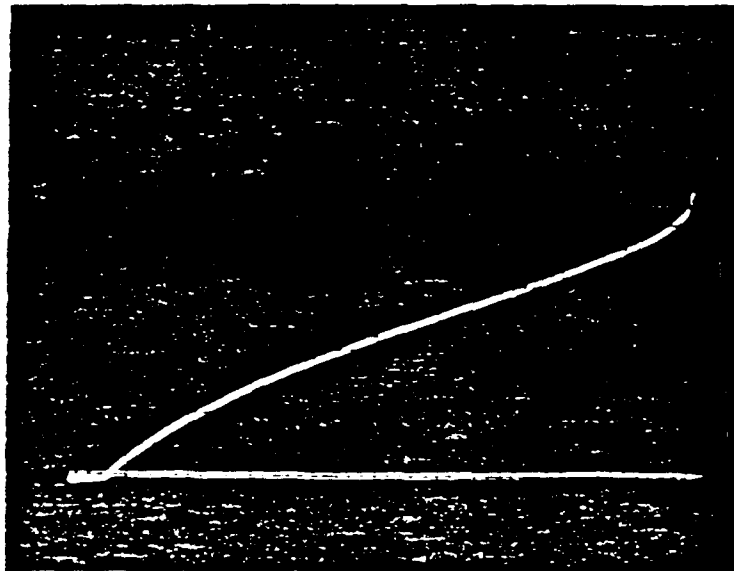
 $\arcsin(x^{1/2})$

Figure 15. Waveform generated by the function generator to drive the multiplier gratings. The horizontal trace at the bottom of the figure is the zero voltage level. Note the section of the curve at the far left of the trace.

EXPERIMENTAL RESULTS

The laboratory equipment setup as previously described is shown in Figure 16. The multiplier gratings were driven at 49 Hz with a peak voltage of ~45 volts. The mirror grating had a d.c. voltage of 45.4 volts applied to it. Figure 17 shows the diffracted orders that arise from each of the gratings. In the laboratory, the function generator voltage was applied to grating M_1 and a D.C. voltage to A_1 with grating M_2 disconnected. The detector was then set to detect beam M_{20} in Figure 17. The oscilloscope trace of that detected signal is shown in Figure 18. Notice that the detected amplitude ramps linearly with x over most of the excursion range. Next, grating M_2 was connected to the function generator and the signal labeled "output" in Figure 17 was detected. This signal is shown in Figure 19. Finally, the device output was connected to a comparator circuit shown in Figure 20. The output of this circuit was monitored on the oscilloscope. The trace in Figure 21 shows the output of the comparator given the detected power from the first diffracted order of the third grating (a_1x^2) and a d.c. voltage ($-a_0$). The point where the curve crosses the horizontal trace (representing 0 volts) corresponds to the value of x for which,

$$a_1x^2 - a_0 = 0.$$

Now, it is a matter of determining the value of " a_1 " (which comes from the diffraction of the adder grating) and knowing the value of " a_0 " (the value of the d.c. input to the op-amp circuit). The value of x can be read directly off of the function generator and by substituting the values of a_1 , a_0 and x into the above equation, the accuracy of the device may be determined.

Laboratory Setup

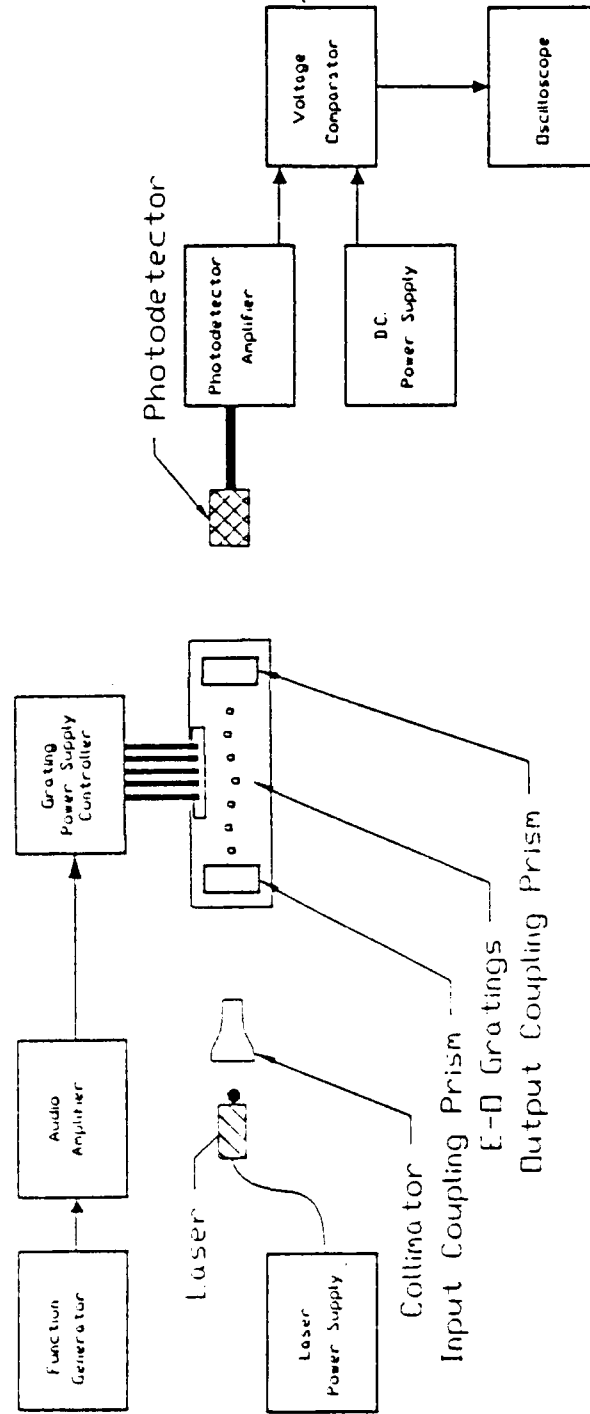


Figure 16. The laboratory setup used in the experiments.

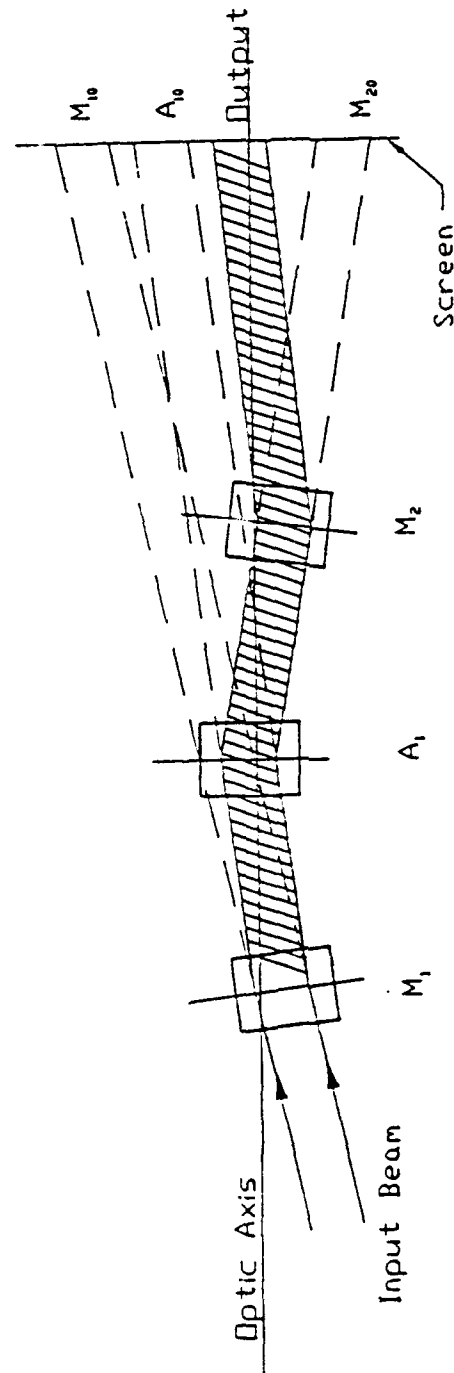


Figure 17. The undiffracted zeroth and first diffracted orders for the three gratings are shown. The subscripts (1) associated with the beams on the screen represent the grating (1) and diffraction order (1) that the beam represents.

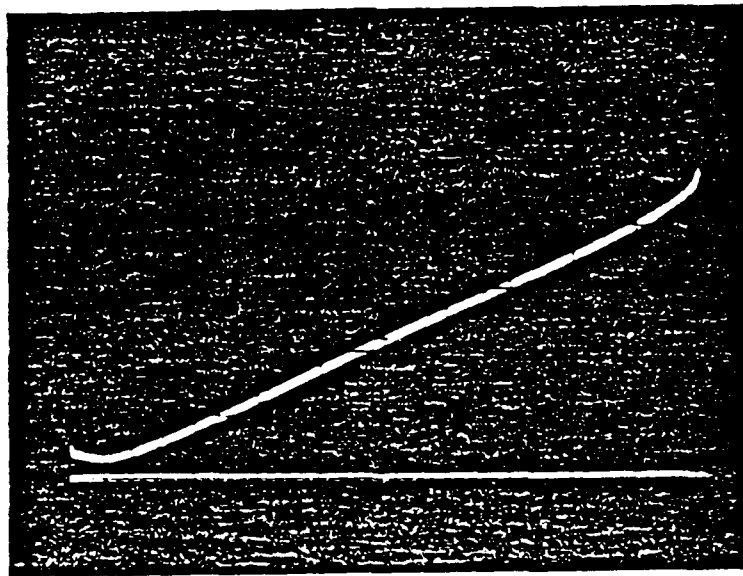


Figure 18. Oscilloscope trace of beam A_{11} (or M_{20}) with grating M_2 turned off. The horizontal trace in the figure represents the zero level.

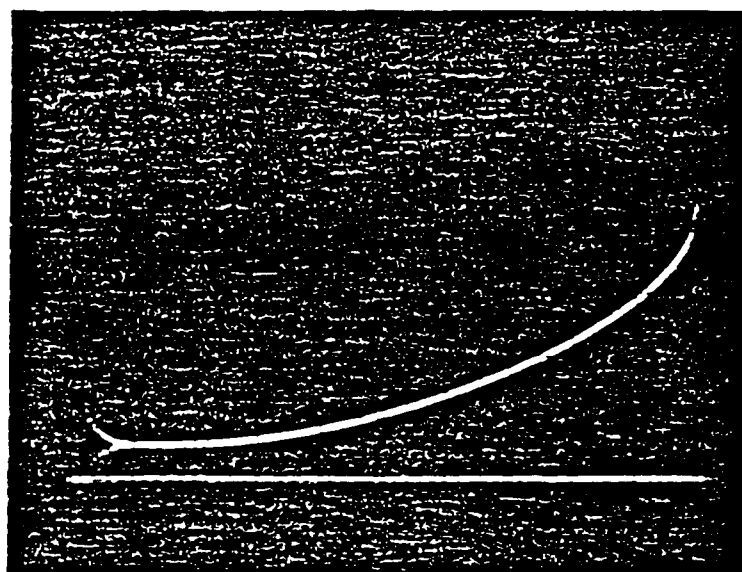


Figure 19. Oscilloscope trace of the first diffracted order from the second multiplier grating. The ringing at the left is due to the detector. Lower trace: zero-voltage level.

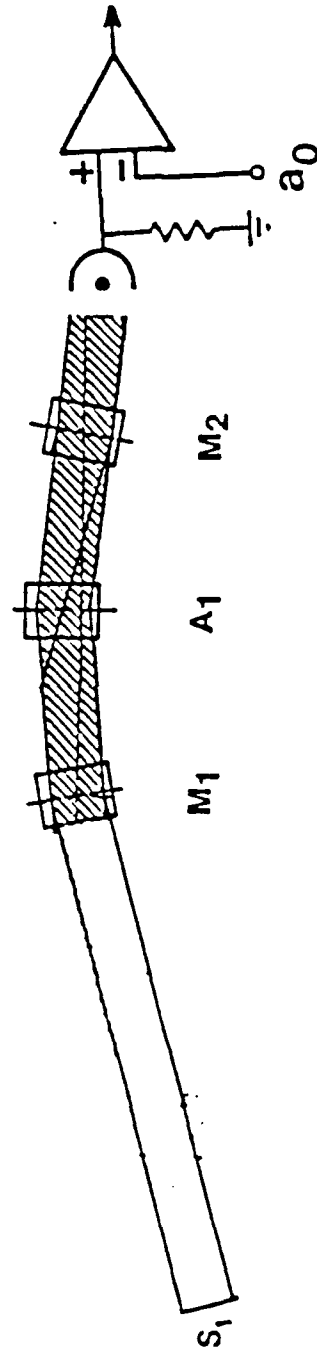


Figure 20. Simplified layout of square root experiment. The $a \cdot x^2$ output of the device is detected and input to the comparator circuit where it is compared to a known d.c. voltage. The output of the comparator is displayed on an oscilloscope.

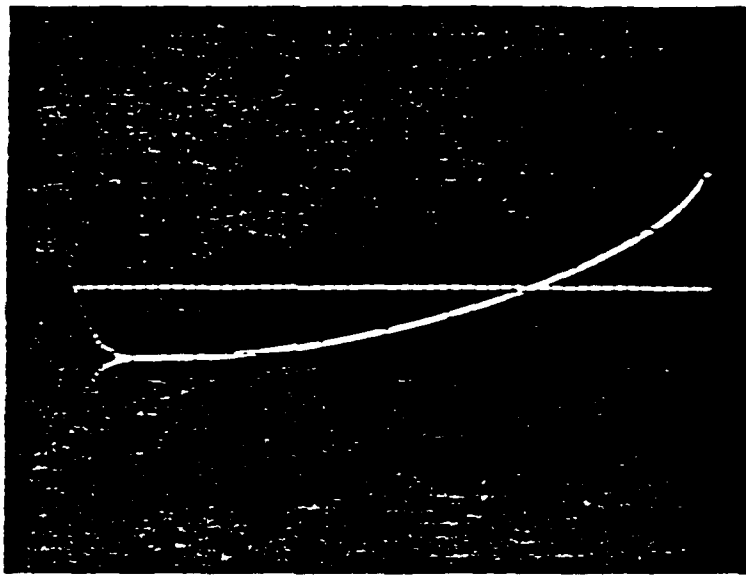


Figure 21. Oscilloscope trace showing adjustment of the d.c. level to set the zero of the output signal.

RE-DESIGN FOR Y-CUT CRYSTALS

Following the discovery that an error had been made in the mask design, resulting in the restriction of beam width to 0.5 mm, and in consideration of the difficulties and high voltages required to operate using a z-cut crystal, it was decided to evaluate the possibility of redesigning the processor mask for operation on a y-cut crystal. In this section, we discuss the tradeoffs involved in the redesign and the actual redesigned parameters of the mask.

DESIGN TRADEOFFS

Selection of y-Cut Crystals

In moving away from the use of z-cut LiNbO_3 , we could use either x-cut or y-cut crystals. The operation of the device on either crystal cut would be the same: the refractive indices, electrooptic coefficients and quality of waveguides are basically the same for the two cuts, especially since the system axis would align with a principal axis of the uniaxial crystal. The selection of y-cut crystals was made on the basis of device size alone: it is difficult to grow crystals of LiNbO_3 both sufficiently free of striations for low-loss waveguiding and sufficiently large for this application. On the contrary, large y-cut crystals of excellent quality are routinely grown and available. There were no other criteria considered.

Propagation Direction and Polarization

For butt-coupled laser-diode coefficient sources, as pointed out earlier, it is important that the low-divergence direction of the laser output - that is, the plane of the junction - be oriented normal to the waveguide plane. For the Sharp laser diodes, the light is polarized with the electric field in the plane of the diode junction, so this requirement would dictate the use of TM modes. However, the planned use of external optics and an external coupling jig relieves us of this requirement, and we are able to use TE light. This is an advantage for two reasons:

- The TE modes of optical waveguides are much less sensitive to the presence of metal electrodes on the waveguide surface than are the TM modes. This is partly due to the fact that the TM modes, but not the TE modes, couple strongly to surface plasmons in the metal. This means that the buffer layer between the surface electrodes and the waveguide surface can be made thinner. This results in better overlap between the applied field and the optical field, and therefore to a lower operating voltage.
- The electrooptic gratings can utilize the r_{33} electrooptic coefficient and an electric field tangential to the surface of the guide. This also leads to lower operating voltage, because r_{33} is large and because the tangential field is continuous across the interfaces. The TM mode, in contrast, utilizes only the smaller r_{22} and r_{13} coefficients; further, E_y is normal to the guide and is significantly diminished on passage into the waveguide because of the relatively high dielectric constant of LiNbO_3 .

These considerations lead to the choice of y-cut, x-propagating TE modes.

Anisotropic Diffraction

The only disadvantage to the use of TE modes in y-cut crystals is that the refractive index of the modes depends upon the propagation direction. This means that the diffraction by the gratings is anisotropic. However, this is a problem only at the design level, and not a significant one there. The design can proceed as if the guide were isotropic, then corrected afterwards by recalculating the grating period and the orientation of its \mathbf{K} vector. In practice, the change in period is far too small to be significant for electrooptic gratings. The change in orientation of \mathbf{K} , while small, is very significant, but easily calculated. It should be noted that only the diffraction from the adder gratings is anisotropic; the multiplier gratings are untilted; so, at Bragg incidence, the diffraction is isotropic.

Because of this design-process simplicity, the presence of anisotropic diffraction at the adder gratings was considered a minor inconvenience.

REDESIGN PARAMETERS

The Redesign Process

The principal redesign effort, once the tradeoffs of the last section were considered, consisted of first modifying (and correcting the segment that led to the error in the first mask) an already-designed spreadsheet template to incorporate the anisotropic diffraction and then calculating the new parameters. Because both a TM mode in a z-cut crystal (first design) and a TE mode in a y-cut crystal (redesign) correspond to the extraordinary polarization for the crystal, no change in the effective mode index was needed, nor were any changes needed in the target period and angular relations for the gratings. The design procedure, then, was to calculate the mask parameters as if the crystal were isotropic, then calculating the change in period and orientation for the adder gratings.

The main burden of the redesign process was to ensure, to the best degree possible, that the design parameters were correct. To do this, the parameters for grating position and rotation angle were used to generate an AutoCad^{*} drawing. Greatly magnified views of this drawing were viewed and printed to ensure accurate passing of the beam from one grating to the next. Only when the device was fully examined was the order for the new mask placed.

New Design Parameters

As expected, the calculated change in period was only of order $0.001\ \mu\text{m}$, far too small to affect fabrication of mask or of electrodes. The final change in adder orientation was found to be only about 0.26° . This should be compared with the angular acceptance range for these gratings of about 0.34° . Finally, the offset of the multiplier gratings, erroneously set at $\pm 0.55\ \text{mm}$ in the first mask, was corrected to $\pm 0.276\ \text{mm}$.

The modified data are displayed in Table X, where the changed data are emphasized.

FABRICATION OF NEW PROCESSOR SAMPLES

Upon receipt, the new photomask was shipped to Battelle-Columbus Laboratories with a 3' wafer of y-cut LiNbO_3 . There, waveguides were formed using the procedures

* AutoCad is a registered trade mark of Autodesk, Inc.

developed for y-cut guides and processor-electrode samples were placed for initial testing. Al electrodes were used to reduce the perturbation on the unbuffered waveguide modes. It was found that, while the losses due to the electrodes were small, there was a tendency for the guided beams to break up. Hence, a thin buffer layer of SiO_2 was placed on the guides and annealed. The resulting processor samples were tested, with the results listed below:

1. All gratings showed diffraction efficiency $> 95\%$.
2. The voltages required were significantly lower than those needed for the z-cut samples.
3. The gratings are aligned properly, and correct handoff was observed.

Three samples were prepared, two of which were of good quality. These have been shipped to Georgia Tech for processor-operation evaluation.

Table X. Final Device Parameters

General Data:

Operating Wavelength	0.783 μm
Substrate Index	2.1784
Surface Index	2.1834
Superstrate Index (Designed for no buffer)	1.0
Effective Index of Guided Mode	2.1799
Electrooptic Coefficient	$3.05 \times 10^{-5} \mu\text{m/V}$
Fill Factor	0.3

Multiplier Grating Data:

Bragg Angle	2.0 deg
Period	5.14 μm
Depth (Finger Overlap)	1.00 mm
Height	1.20 mm
Nath parameter @100% d.e. ($\approx 16.75 \text{ V}$)	27

Adder Grating Data:

Bragg Angle	1.7 deg
Period	6.06 μm
Depth (Finger Overlap)	1.00 mm
Height	1.20 mm
Nath parameter @ 100 % d.e. ($\approx 19.65 \text{ V}$)	20

Grating Placement Data:

Spacing between adder gratings on S.A.	15.76 mm
Center of first adder on SA (A_0)	10.628 mm
Center of second adder on SA (A_1)	26.389 mm
Center of third adder on SA (A_2)	42.150 mm
Center of fourth adder on SA (A_3)	57.911 mm
Tilt angle of adder gratings	$\pm 3.45 \text{ deg}$
Vertical offset of multiplier gratings	$\pm 0.276 \text{ mm}$
Center of first multiplier grating (M1)	18.509 mm
Center of second multiplier grating (M2)	34.270 mm
Center of third multiplier grating (M3)	50.031 mm

Source Spacing Data:

Position of first source (S_0)	1.00 mm
Spacing between sources	2.96 mm

Anisotropic Diffraction Data:

Change in adder-grating tilt angle	0.2556 deg
Change in adder-grating period	0.001 μm

LIST OF SYMBOLS

θ_{BA}	Bragg angle for "adder" gratings.
θ_{BM}	Bragg angle for "multiplier" gratings
θ_0	Angle between coefficient beams and system axis
SA	System Axis
ρ	Nath parameter for gratings
λ_0	Vacuum wavelength of light used
Λ	Grating Period
n_0	Average refractive index in grating region
n_1	refractive-index modulation comprising the grating
η	diffraction efficiency for general incidence
η_B	diffraction efficiency at Bragg incidence
ν	dimensionless parameter (determines η_B)
ξ	dimensionless parameter (detuning from θ_B)
ϑ	dephasing factor
X_{Ai}	x-coordinate (along SA) of center of adder # i
X_{Mi}	x-coordinate (along SA) of center of multiplier #i
Y_{Mi}	y-coordinate (from SA) of center of multiplier #i
S	spacing between coefficient beams
S_i	position of i-th coefficient source, measured from origin along perpendicular to the coefficient beams:

$$S_1 = S_3 + S; \quad S_2 = -S; \quad S_4 = -2S$$

h_A = height of an adder grating (number of periods times the length of a period)

h_M = height of a multiplier grating

w, W = the width of the optical beam

REFERENCES

1. Carl M. Verber, R.P. Kenan, H. John Caulfield, Jacques E. Ludman and P. Denzil Stilwell, Jr., "Pipelined Polynomial Processors Implemented with Integrated Optical Components". *Appl. Opt.* vol. 23 No.6, pp. 817-821, 1984.
2. R.P. Kenan and C.M. Verber, "Integrated Optical Pipeline Processor", in *Optical and Hybrid Computing*, SPIE Institutes for Advanced Optical Technologies, 24-27 March, 1986, Leesburg, VA., SPIE Vol. 634, pp.393-408.
3. Richard P. Kenan, "Theory of Crossed-Beam Diffraction Gratings", *IEEE J. Quantum Electron.*, vol. QE-14, pp. 924-930, 1978.
4. H. Kogelnik, "Coupled Wave Theory for Thick Hologram Gratings", *Bell Syst. Tech. Jour.*, vol. 48, pp. 2909-2947, 1969.
5. Yim-Kul Lee and Richard P. Kenan, "Four-Wave Theory of electrooptic Gratings with a Simple Expansion for Use in Design", *Appl. Opt.*, vol.28, #1, pp.74-81, January, 1989.

**MISSION
OF
ROME LABORATORY**

Rome Laboratory plans and executes an interdisciplinary program in research, development, test, and technology transition in support of Air Force Command, Control, Communications and Intelligence (C³I) activities for all Air Force platforms. It also executes selected acquisition programs in several areas of expertise. Technical and engineering support within areas of competence is provided to ESD Program Offices (POs) and other ESD elements to perform effective acquisition of C³I systems. In addition, Rome Laboratory's technology supports other AFSC Product Divisions, the Air Force user community, and other DOD and non-DOD agencies. Rome Laboratory maintains technical competence and research programs in areas including, but not limited to, communications, command and control, battle management, intelligence information processing, computational sciences and software producibility, wide area surveillance/sensors, signal processing, solid state sciences, photonics, electromagnetic technology, superconductivity, and electronic reliability/maintainability and testability.